REVIEW

An introductory review of the thermal structure of subduction zones: I. Motivation and selected examples

Peter E. van Keken* and Cian R. Wilson

*Correspondence:
pvankeken@carnegiescience.edu
Earth and Planets Laboratory,
Carnegie Institution for Science,
5241 Broad Branch Road, NW,
Washington DC 20015, USA.
Full list of author information is
available at the end of the article

Abstract

The thermal structure of subduction zones is fundamental to our understanding of physical and chemical processes that occur at active convergent plate margins. These include magma generation and related arc volcanism, shallow and deep seismicity, and metamorphic reactions that can release fluids. Computational models can predict the thermal structure to great numerical precision when models are fully described but this does not guarantee accuracy or applicability. In a pair of companion papers the construction of thermal subduction zone models, their use in subduction zone studies, and their link to geophysical and geochemical observations is explored. In part I the motivation to understand the thermal structure is presented based on experimental and observational studies. This is followed by a description of a selection of thermal models for the Japanese subduction zones.

Keywords

Geodynamics, Plate tectonics, Finite element methods, Subduction zone metamorphism, Arc volcanism

1 Introduction

Subduction zones are tectonically active regions on Earth where oceanic plates descend into the Earth's mantle below a continental or oceanic plate. These are locations that experience explosive arc volcanism, large underthrusting earthquakes along the seismogenic zone, and continental crust production. Deeper expression of subduction are, for example, the metamorphic changes that include dehydration reactions that lead to melting in the overlying mantle and that can lead to intermediate-depth and deep seismicity (Figure 1a).

The thermal state of subduction zones exerts fundamental controls on volcanic activity, seismicity, and metamorphic reactions. We will provide an introductory overview of observational, experimental, and modeling approaches that can be used to understand the thermal structure of subduction zones and its impact on global dynamics. We have provided a broad discussion with more detail than is common in review papers. This is intended to broaden the appeal of this review to an audience of advanced undergraduate students, graduate students, and any professionals from outside the field of geodynamics who are interested in an introductory review. We will focus on modeling details that allow readers to better comprehend how subduction zone thermal models are formulated, executed, and validated. We will discuss recent literature in particular to highlight the broad and current interest that the

Figure 1 Subduction zone processes and example of thermal structure. a) Cartoon of subduction zone processes that control and are affected by its thermal structure (modified from van Keken (2003)). b) Thermal structure predicted for Tohoku (trench-perpendicular cross-section below Sendai, Miyagi Prefecture) adopted from van Keken et al. (2012)). T is temperature. Contour lines are shown at every 100°C. At the decoupling depth d_c the slab changes from decoupling at shallower depths to full coupling with the overlying mantle wedge. Note that we use the terms coupling and decoupling here and elsewhere in their long-term geodynamical context. This is in contrast with the context of the frictional-elastic seismic cycle at shorter time scales where these terms are used in the opposite sense. Green line: oceanic Moho. Black top line indicated by M is the continental Moho. This cross-section shows the predicted thermal structure for an end-member cold subduction zone which is caused by the rapid (8.3 cm/yr) subduction of old (130 Myr) oceanic lithosphere. c) Temperature of the top of the oceanic crust (in red) and oceanic Moho (in green) as a function of lithostatic pressure P and depth.

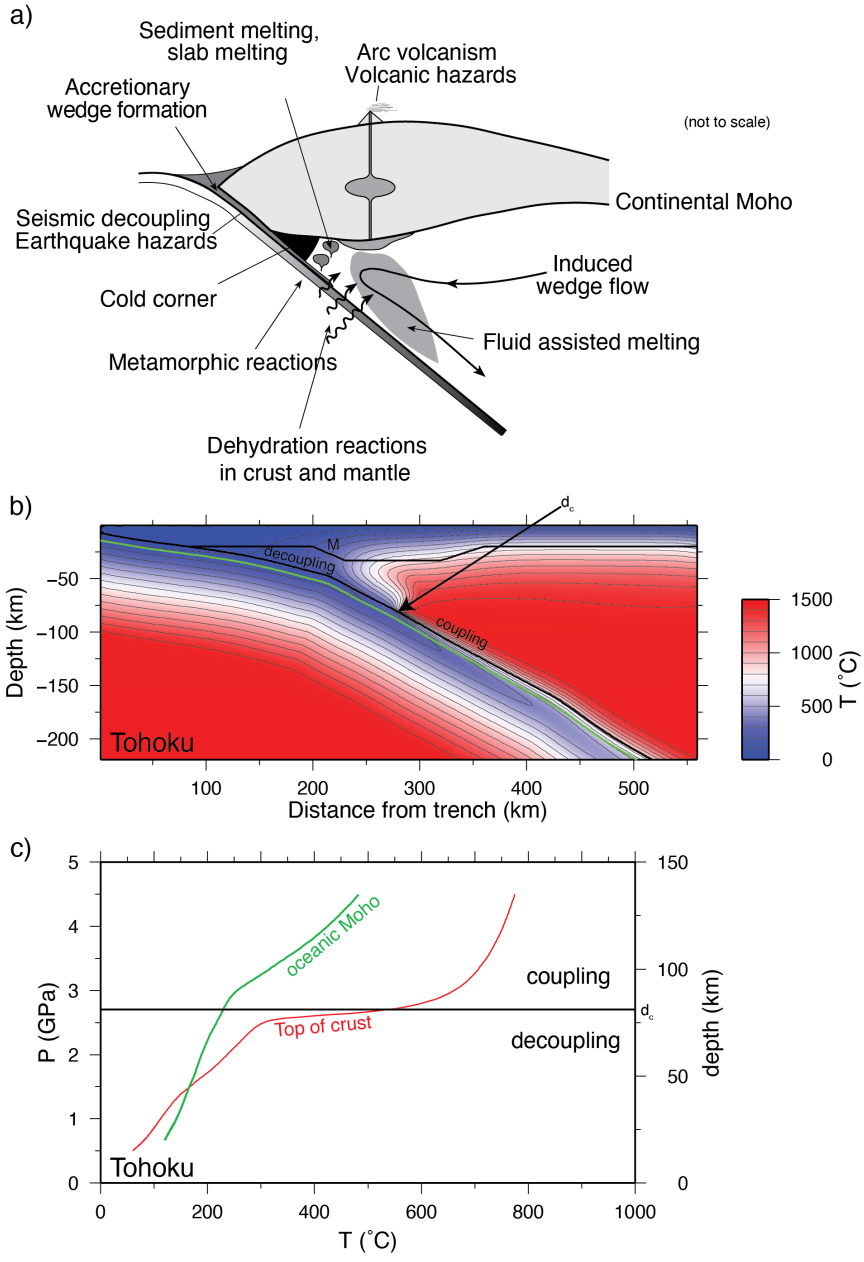

solid Earth scientists have in the thermal structure of subduction zones. For more

"traditional" reviews see van Keken (2003), Wada and King (2015), and Peacock (2020).

1.1 Mechanisms and factors controlling thermal structure

The oceanic lithosphere is a rheological boundary layer of the Earth's solid mantle that is relatively strong compared to the underlying asthenosphere. The lithosphere has petrological distinctions with a ∼6 km thick crust (Christeson et al., 2019) that overlies a depleted layer of harzburgite from which the melt that formed the crust at mid-oceanic ridges has been extracted. As the oceanic lithosphere spreads from the mid-ocean ridge it ages and cools; at an age of 80–100 Myr the lithosphere reaches a typical thickness of 100 km. Upon subduction, the oceanic lithosphere stops cooling and starts warming due to a combination of processes. Along its entirety, the slab warms due to heat flowing from the warm mantle at the base of the slab. At shallow depths (less than ∼50 km) radiogenic heat produced in the crust of the overriding plate and shear heating due to friction along the plate interface can heat the top of the slab (e.g., Molnar and England, 1990; van Keken et al., 2019). In most present-day subduction zones, the slab appears to remain decoupled (over long geodynamical time scales) from the overriding mantle to a depth of 75–80 km forming a "cold corner" in the mantle wedge (Furukawa, 1993; Wada and Wang, 2009, Figure 1a). Below this depth the slab couples to the overriding mantle wedge asthenosphere (Figure 1b). The motion of the subducting plate results in a drag on the overlying mantle that leads to a cornerflow, which causes advective transport of the hot mantle wedge material onto the slab that in turn provides rapid warming of the slab surface and of the underlying oceanic crust and mantle by further conduction.

The dramatic heating of the slab surface below the coupling depth (indicated by d_c in Figure 1) is evident by the tightening of the isotherms near the slab surface (Figure 1b) and the rapid heating of the slab surface (Figure 1c). While the oceanic Moho (green line in Figure 1b) is only ∼6 km from the top of the oceanic crust, the temperature increase here is modest and lags significantly behind that at the top. The average temperature gradient can be more than 50°C/km throughout the subducting crust. The conductive heat flow from the top is in competition with the advective transport of the cold slab that originates at the trench. As a consequence, one can predict that metamorphic reactions (including those involving dehydration) occur at very different depths in the slab as it descends into the mantle.

Important primary factors that control the thermal conditions in subduction zones at depth are the age of the incoming plate, the descent rate (which is controlled by the convergence velocity at the trench and slab geometry), the frictional properties of the shear zone decoupling the slab from the overriding plate, and, at greater depth, the rheology of the mantle wedge that controls the corner flow. The first two parameters are used in the subduction zone thermal parameter Φ which is defined as the multiplication of age at the trench in Myr, convergence speed in km/Myr, and the sine of the (average) dip of the slab geometry (Kirby et al., 1996). The first two can be readily found for a given subduction zone section from global databases (see approach discussed in Syracuse and Abers, 2006). The dip dependence of Φ is useful if one wishes to estimate how fast the thermal effect of

subduction along a straight plane reaches a particular depth. Syracuse and Abers (2006) determined the average dip for any of their 51 subduction zone segments by averaging the dip within the 50 to 150 km depth contours (Ellen Syracuse, personal communication). This approach was also used in determining the average dip for the expanded selection of 56 subduction zone segments used in Syracuse et al. (2010). It should be noted that this parameter is the most uncertain in Φ since it can vary greatly depending on specific cross-section and the method used to determine average dip. Since most subduction zones show a change from shallow dip at the trench to intermediate or large dip at depth one should not be overly confident in applying the thermal parameter – it might be more useful to consider a simplified thermal parameter that is just age times convergence speed.

The thermal parameter (simplified or not) is a useful indicator whether we might expect a subduction zone to be on the "warm" or "cold" end of the spectrum or that it may be more "intermediate". For example, using the Syracuse et al. (2010) compilation, Cascadia (Φ=100 km) and Nankai (Φ=450 km) are by this criterion among the warmest subduction zones whereas Tohoku and Hokkaido ($\Phi\sim$6000 km) and in particular Tonga (Φ=14,800 km) are among the coldest. Cascadia and Tonga occupy the extremes – the average and median values for Φ are 2900 km and 2200 km, respectively. It should be noted that the current value for Tonga is higher than that in Syracuse and Abers (2006) who estimated Φ=6300 km. The difference is because Syracuse et al. (2010) took into account the addition of the high trench retreat velocity due to the opening of the Lau backarc basin. An example that shows a moderate correlation between Φ and slab temperatures at the top of the slab is in van Keken et al. (2011, their Figure 2). By contrast, Figure 12F in Syracuse et al. (2010) showed little correlation between the sub-arc slab surface temperature and thermal parameter. There is no internal discrepancy here – the models used in these two papers are largely similar. The reason for the scatter in the temperature at the slab surface below the arc is that this part of the slab surface is still seeing a rapid temperature increase due to the mantle wedge flow whereas at 120 km depth the temperature increase is significantly more gentle (Figure 1c). This clearly suggests that Φ in either of its forms should be used with caution when discussing processes that occur below the arc.

1.2 Why do we need to know the thermal structure of subduction zones?

Before we start a discussion on how we can formulate subduction zone thermal models it may be useful to consider why we might be interested in this in the first place. We will provide a motivation by highlighting work from the last decade or so that use model estimates from compilations of global models as presented, for example, by Wada and Wang (2009) and Syracuse et al. (2010) to inspire experiments or interpret geochemical and geophysical observations that are relevant to our understanding of the dynamics of subduction zones. We embark on this section with some trepidation as any conclusions and interpretations presented here may only be as strong as the thermal models they are based on.

1.2.1 Design and interpretation of physical experiments

Global compilations of subduction thermal structure have been used extensively to determine whether experimentally determined metamorphic changes and melting under various hydration states can occur in present-day subduction zones and

whether they can explain volcano geochemistry. For example, Tsuno et al. (2012) determined that the sub-volcano slab surface below Nicaragua could not produce carbonated sediment melting but that carbonitite production could occur in the warmer overlying wedge after diapiric rise. Jégo and Dasgupta (2013, 2014) used thermal model constraints to show that sulfur could be transferred from the slab to mantle wedge either by aqueous fluids or by melting of the hydrated basaltic crust. Brey et al. (2015) used global estimates to constrain experimental conditions of carbonate melting in the presence of graphite or diamond. A similar approach was taken by Merkulova et al. (2016) but now for studying the role of iron content on serpentinite dehydration. Lee et al. (2021) used thermal models of cold subduction zones to argue for the stability of chloritoid and its contribution to the relatively strong trench-parallel seismicity observed in such regions.

Bang et al. (2021) used thermal models to study the stability of subducted glaucophane over Earth's thermal evolution. Codillo et al. (2022) showed chlorite is preferentially formed over talc during Si-metasomatism of ultramafic rocks while also suggesting a limited rheological role of talc in determining the physical structure of subduction zones (as suggested to the contrary by Peacock and Wang, 2021). Martindale et al. (2013) used models specific for the Marianas subduction zone to design experiments focusing on high-pressure phase relations of volcaniclastic sediments and demonstrated that these sediments contribute widely to the geochemical characteristics of Mariana arc magmas. The global spread of the predicted subduction zone thermal structures has also been used to understand the phase stability field of various serpentinite phases and to rule out that a laboratory-produced high-pressure form of antigorite could be stable inside the Earth (Reynard, 2013).

1.2.2 Interpretation of geochemistry

Thermal models have been used to interpret processes that contribute to geochemical heterogeneity seen in arc lavas. Examples include those exploring the relationship between geochemical signatures of the subducting slab and arc volcanism (Rustioni et al., 2021) as well as the mechanisms causing volcanism (Marschall and Schumacher, 2012). Global models provided the suggestion that aqueous fluids and hydrous melts produced enhanced chemical recycling particularly in hot subduction zones (Hernández-Uribe et al., 2019). Applications to specific elemental or isotopic systems include those of Ce and Nd under the Mariana volcanic arc (Bellot et al., 2018) and the determination that nitrogen subduction in clay minerals is only possible in cold subduction zones (Cedeño et al., 2019). Slab surface temperatures strongly correlate with Mg isotope ratios observed in volcanic arcs confirming a thermal control on processes controlling Mg release from the subducting slab (Hu et al., 2020). In a more regional example, slab surface temperatures in the Lesser Antilles are predicted to be lower than that required for slab melting, suggesting the role of dehydration of the slab crust (including sediments) as indicated for example from K isotopic studies (Hu et al., 2021). Vho et al. (2020) used the average subduction zone thermal structure to model oxygen isotope variations to study fluid-rock interaction. They suggested the potential for rapid serpentinization of the forearc mantle by slab fluids and that the use of oxygen isotopes allows fluid pathways, the type of flow, and pressure-temperature conditions encountered by the fluid to be tracked.

Thermal models of the subducting slab such as those in van Keken et al. (2002) and Syracuse et al. (2010) form a fundamental part of geochemical modeling applications facilitated by the Arc Basalt Simulator suite of tools (Kimura, 2017; Kimura et al., 2009). A few examples of the many applications of these tools are as follows. Mazza et al. (2020) found that the slab thermal structure controls release of tungsten and its isotopic ratios which allows for tracing of slab dehydration and slab melting. Kimura et al. (2014) showed that the wide diversity of magma types found through SW Japan in response to the subduction of the young Philippine Sea Plate was caused by melting of the slab and that this induced flux melting of peridotite in the mantle wedge. A combined geochemical and geophysical study explored the role of water in magma genesis in the much colder NE Japan subduction zone and allowed for mass balance constraints on local water fluxes (Kimura and Nakajima, 2014). Variations of arc lava composition between the volcanic arc and backarc in the northern Izu arc could be explained by differences in the pressure and temperature conditions during melting in addition to variable water content (Kimura et al., 2010).

1.2.3 Translation of mineral physics to geophysical quantities

Slab thermal models are routinely used in interpreting how the presence of volatiles could affect geophysical properties predicted from laboratory experiments (e.g., Förster and Selway, 2021; Huang et al., 2021; Pommier et al., 2019). This allows for the interpretation of the role of fluids in explaining electromagnetic and magnetotelluric observations over subduction zones (Förster and Selway, 2021; Pommier and Evans, 2017). Chen et al. (2018) used thermal model predictions for various regions to understand the role of phengite dehydration on the formation of high conductivity anomalies above subducting slabs. Similar studies focused on the influence of dehydration on the electrical conductivity of epidote (Hu et al., 2017), talc (Wang et al., 2020), NaCl-bearing aqueous fluids (Guo and Keppler, 2019), and glaucophane (Manthilake et al., 2021).

1.2.4 Plate interface earthquakes, slow slip, and episodic tremor

Global thermal models have also been used to explore seismic processes occurring at the plate interface below the forearc, which include the seismogenic zone that experience underthrusting seismic events (such as the 2011 Tohoku-oki earthquake) that are separated by interseismic periods. Understanding the rheological properties of the plate interface, for example whether the plate interface is locked or deforms by aseismic creep (see, e.g., Loveless and Meade, 2011), is essential to understand the seismic hazards in a particular subduction zone. The discovery of episodic tremor and slip (e.g., Rogers and Dragert, 2003) and its relation to low-frequency earthquakes (Shelly et al., 2006) has led to a further appreciation of the important role of rheology and fluid production along the plate interface. These processes are both at least in part temperature-dependent and it is expected that various features of the plate interface are controlled by the thermal characteristics of a given subduction zone. As an example, use of specific thermal models showed a relatively low temperature (less than 300°C) at the down-dip limit of the seismogenic zone (Fagereng et al., 2018). In a study combining field examples of sand-shale mélanges from Kodiak accretionary complex and the Shimanto belt with kinematic modeling, Fisher

et al. (2019) demonstrated the strong influence temperature at the slab top has on the healing of cracks that modulate the fault zone strength during the interseismic period. The Syracuse et al. (2010) model for Tohoku was used as a basis for models explaining the viscoelastic flow after the 2011 Tohoku-oki earthquake (Agata et al., 2019). Condit et al. (2020) showed from warm subduction zone models that locally produced fluids are sufficient to explain episodic tremor and slip events.

1.2.5 Nature of intermediate-depth and deep seismicity

Earthquakes in the shallow crust and mantle as well as underthrusting events along the seismogenic zone tend to be caused by brittle failure, which is possible due to differential stresses under modest hydrostatic pressures. At depths greater than ∼40–70 km the hydrostatic pressure becomes large enough to make brittle failure ineffective, which therefore requires different physical mechanisms to cause intermediate-depth (∼70–400 km) and deep (∼400–700 km) earthquakes (see Frohlich, 2006). Intriguingly, intermediate-depth seismicity seems to have a strong petrological control as shown by Abers et al. (2013). In cold subduction zones such as Tohoku and Hokkaido the upper plane seismicity of the Wadati-Benioff zone peaks in the oceanic crust (Figure 2a). The oceanic crust in warm subduction zones tends to have little seismicity in the oceanic crust with seismicity peaking in the slab mantle (Figure 2b). Abundant seismicity and dense seismic networks allow for precise hypocenter locations below Japan (e.g., Kita et al., 2010b). Thermal modeling suggests that the major dehydration reaction of blueschist to lawsonite eclogite facies (informally denoted as the "blueschist-out" boundary; Figure 2c) occurs at a pressure and temperature range just where seismicity in the upper plane disappears (van Keken et al., 2012, Figure 2d). This strongly suggests that fluids caused by dehydration of blueschist facies rock travel back up the slab triggering the shallower seismicity, possibly through hydrofracturing caused by fluid overpressure (Padrón-Navarta et al., 2010). The presence of free fluids in parts of the oceanic crust below Tohoku that have abundant seismicity is strongly suggested from observations of very low P-wave speeds in seismically active region of the subducting crust below Tohoku (Shiina et al., 2013, Figure 2e) and Hokkaido (Shiina et al., 2017).

Sippl et al. (2019) interpreted the seismicity distribution in the Northern Chile subduction zone to be caused by the production of fluids due to metamorphic dehydration reactions triggered by heating when the slab gets into contact with the hot mantle wedge. In this region, Bloch et al. (2018) demonstrated a correlation between earthquakes and a high V_p/V_s region in the lower plane of the double seismic zone that is likely due to antigorite dehydration at depth and the presence of fluids at shallower depths. Wei et al. (2017) showed that the double seismic zone in Tonga extends to a maximum depth of 300 km with a clear trend of the maximum depth along a given profile correlating with the convergence speed, suggesting that metamorphic dehydration, likely that of antigorite, occurs when the slab interior first reaches ∼500°C.

Independent support for the role of free fluids in the subducting oceanic crust is provided by modeling of fluid flow in subduction zones where the (important, but often ignored) driving force of pressure gradients caused by compaction of rock upon dehydration is included. Without this force fluids tend to leave the slab by

buoyancy alone – with compaction pressure fluids released by dehydration reactions in the crust tend to travel back up the subducting crust before exiting the slab (Wilson et al., 2014, Figure 2e). Note that the model with compaction pressure causes the fluids to exit below the arc allowing for a self-consistent explanation of the location of the arc. The broad and distributed fluid release from the slab in the buoyancy-only model would predict multiple volcanic fronts which is generally not observed. The suggestion that distributed seismicity is caused by fluid flow in the slab is an alternative to ideas presented by Ferrand (2019) who used various thermal model estimates of the pressure-temperature conditions in earthquake hypocenters to argue that dehydration of antigorite as well as other hydrous phases causes stress transfer to trigger seismicity. It should be noted that pervasive fluid flow is also evident from field observations of exhumed portions of the oceanic crust (e.g., Bebout and Penniston-Dorland, 2016; Piccoli et al., 2016).

Fluids may also play a critical role in deeper seismicity which forms an alternative to proposed processes such as shear heating instabilities (Kelemen and Hirth, 2007; Prakash et al., 2023). For example, Shirey et al. (2021) explored the correlation between seismicity, dehydration reactions, and diamond formation in cold subduction zones. They argued from thermal modeling that the conditions for deep intermediate-depth seismicity are principally met in cold subduction zones because in these regions the crust and uppermost mantle can bypass shallow dehydration reactions.

Note that seismicity in the subducting slab is generally widely distributed rather than tightly clustered. This appears to be in conflict with the hypothesis that embrittlement due to mineral dehydration reactions is the main cause for intermediate-depth seismicity (e.g., Jung et al., 2004; Raleigh and Paterson, 1965). Dehydration embrittlement would cause earthquakes to be located at the site of dehydration reactions that are in a narrow pressure-temperature range and therefore would cause clustering of earthquakes around these boundaries which is contrary to observations (see also Ferrand, 2019). While heterogeneity, such as the variable presence (and absence) of hydrous phases would create patches rather than (near-)continuous seismicity but this would still occur under specific pressure-temperature conditions if dehydration embrittlement were the main mechanism and would therefore not explain the widely distributed seismicity.

1.2.6 Mobilization and deep cycling of volatiles

Compilations of thermal subduction zone structures have been critically used (along with predictions of metamorphic phase stability and water content as a function of lithology, pressure, and temperature) to understand where fluids are being released from the slab (Cannaò et al., 2020; Hermann and Lakey, 2021; Rüpke et al., 2004; van Keken et al., 2011; Vitale Brovarone and Beyssac, 2014). This applies particularly to the release of H_2O but also to that of carbon by aqueous fluids (Arzilli et al., 2023; Farsang et al., 2021). Tian et al. (2019) used simplified models of thermal structure with a comprehensive thermodynamic parameterization of open system reactive flow in the subducting slab. They showed the importance of redistribution of carbon by fluid flow within the lithological layers and that the subduction efficiency of H_2O and CO_2 is increased by fractionation within the subducting

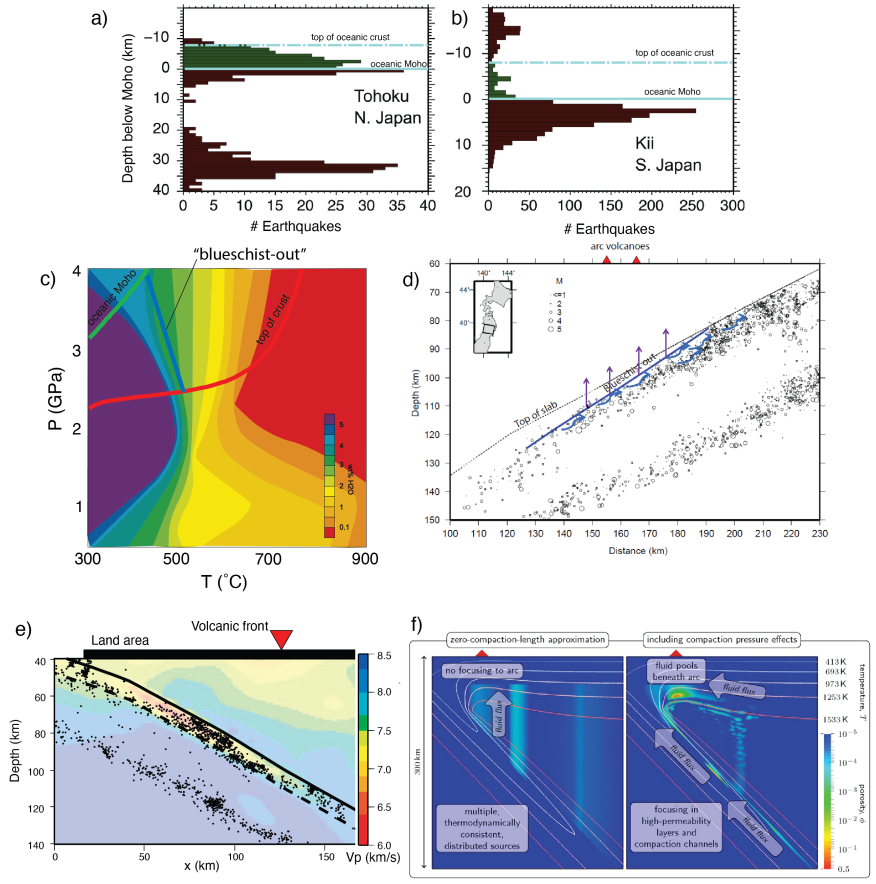

Figure 2 a)-b) Panels showing histogram of earthquakes in crust and mantle for cold and warm subduction zones (modified from Abers et al., 2013). c) Figure showing H_2O carrying capacity in the oceanic crust (modified from Hacker, 2008). The P-T paths at the top of the crust and oceanic Moho from Figure 1c are overlain - bold blue line shows the relevant "blueschist-out" boundary. d) Earthquakes limited by "blueschist-out" below Tohoku with interpreted fluid flow (modified from van Keken et al., 2012). e) Low V_p in crust below Tohoku suggesting presence of free fluids (modified from Shiina et al., 2013). Note that the blue colors in the legend are accidentally rendered as purple in the figure such that the purple region has V_p>8 km/s. f) Figure showing fluid flow rises primarily with gravity if compaction pressure is ignored (left frame); if it is included (right frame) the fluids tend to be contained in the crust before leaving the slab below the arc (modified from Wilson et al., 2014) similar to the flow of fluids suggested from the seismicity (frame d) and low P-wave velocities (frame e).

lithologies. These approaches not only facilitate our understanding of the release of fluids and their contribution to subduction zone processes, but also have been used as input to global models predicting the long term chemical evolution of the Earth's mantle (e.g., Kimura et al., 2016; Shimoda and Kogiso, 2019). In a separate study, Smye et al. (2017) used the global set of thermal models to quantify noble gas recycling into the deep mantle. They showed a correlation between noble gases and H_2O and that strong fractionation occurred in warm subduction zone settings with minimal fractionation in cold slabs.

2 Geophysical observations guiding modeling of the thermal structure of subduction zones

Figure 1a provides a cartoon of subduction zone structure that builds on geophysical observations of heat flow, seismology, and geodetics. Combined, these methods indicate that the mantle wedge is composed of a hot region below the arc and backarc that is fairly sharply delineated from a cold forearc mantle in the tip of the wedge where the slab surface is above ∼80 km depth. This wedge tip has generally been called the "cold corner" or "cold nose" of the mantle wedge that indicates the presence of significant rheological heterogeneity of the slab surface and mantle wedge that directly controls the thermal structure of subduction zones (and can therefore be used to construct thermal models such as the one in Figure 1b). In this section we will explore the main geophysical observations that have led to the concept of the "cold nose" and the partitioning of the mantle wedge into a cold and hot region that is separated by a fairly sharp vertical boundary.

2.1 Heat flow

Early heat flow measurements in the Tohoku subduction zone (see discussion and citations in Honda, 1985) suggested a significant change in heat flow values when moving from the trench to the volcanic arc – very low heat flow values over the forearc are sharply separated from much higher and more scattered heat flow values in the arc and backarc. The scattered values in the arc and backarc regions are likely due to local processes such magma transport in the crust and heterogeneous heat production, as well as potential bias in the continental data (Furukawa and Uyeda, 1989). An updated heat flow database for Japan (Tanaka et al., 2004) shows broad consistency of this pattern along Tohoku and Hokkaido (Figure 3a). Similar observations are now available for many subduction zones, including the Andes (Henry and Pollack, 1988; Springer and Förster, 1998), Cascadia (see compilation in Currie et al., 2004, and Figure 3b), Kermadec (Von Herzen et al., 2001), and Ecuador–Columbia (Marcaillou et al., 2008). Heat flow data are traditionally obtained using Fourier's law by measuring the thermal gradient and rock conductivity in boreholes (Pollack et al., 1993) or by marine heat flow probes (e.g., Hyndman et al., 1979). Alternative methods employ electromagnetic measurements of the Curie point depths and seismic observations of the Bottom-Simulating Reflector (BSR). The first method makes use of change from ferromagnetic to paramagnetic behavior in minerals such as magnetite when rock is heated above the Curie temperature. Determining the depth of this transition therefore allows for estimates of the average thermal gradient in the crust with examples in Mexico (Manea and Manea, 2011), northeast Japan (Okubo and Matsunaga, 1994) and the western Pacific (Yin et al., 2021). The second method measures the location of the base of the stability field of clathrate hydrates which has a well-calibrated temperature and pressure range. Depth determinations of the BSR lead therefore to determinations of temperature gradients and from that estimates for the average heat flow through the shallow crust. Examples of the application of the BSR technique exist for Cascadia (Salmi et al., 2017), Costa Rica (Harris et al., 2010), Hikurangi (Henrys et al., 2003), and Nankai (Hyndman et al., 1992; Ohde et al., 2018).

Figure 3 a)-b) Heat flow measurements over subduction zones show a marked low heat flow in the forearc, transitioning to higher and more scatted observations in the arc and backarc (where the slab is at a depth of greater than 80 km). a) Heat flow measurements for Tohoku. Solid blue triangles show average heat flow for Tohoku as a function of trench distance; solid circles: same but now for heat flow measurements within 100 km distance from the profile T18 from van Keken et al. (2002) shown in Figure 1. b) Heat flow measurements from the global heat flow database (see Pollack et al., 1993, and https://www.geophysik.rwth-aachen.de/IHFC/heatflow.html) near the CAFE profile in Cascadia (Abers et al., 2009). The high heat flow near the trench is due to the young age of the subducting lithosphere. c)-e) Seismic attenuation studies in Central Alaska (modified from Stachnik et al., 2004) show a sharp transition between attenuating properties of the forearc and arc/backarc mantle c) Waveforms observed for an earthquake recorded in a station over the arc. d) Same as c) but now for waveforms obtained for the same earthquake by a station located over the forearc. Note the significant change in amplitude scale as well as the change in frequency content of the waveforms between the two recordings. e) Attenuation tomography showing a sharp transition between high Q in the forearc mantle wedge and low Q elsewhere. Raypaths of the earthquake to stations with waveforms recorded as shown in panel c) and d) are schematically indicated with the arrows.

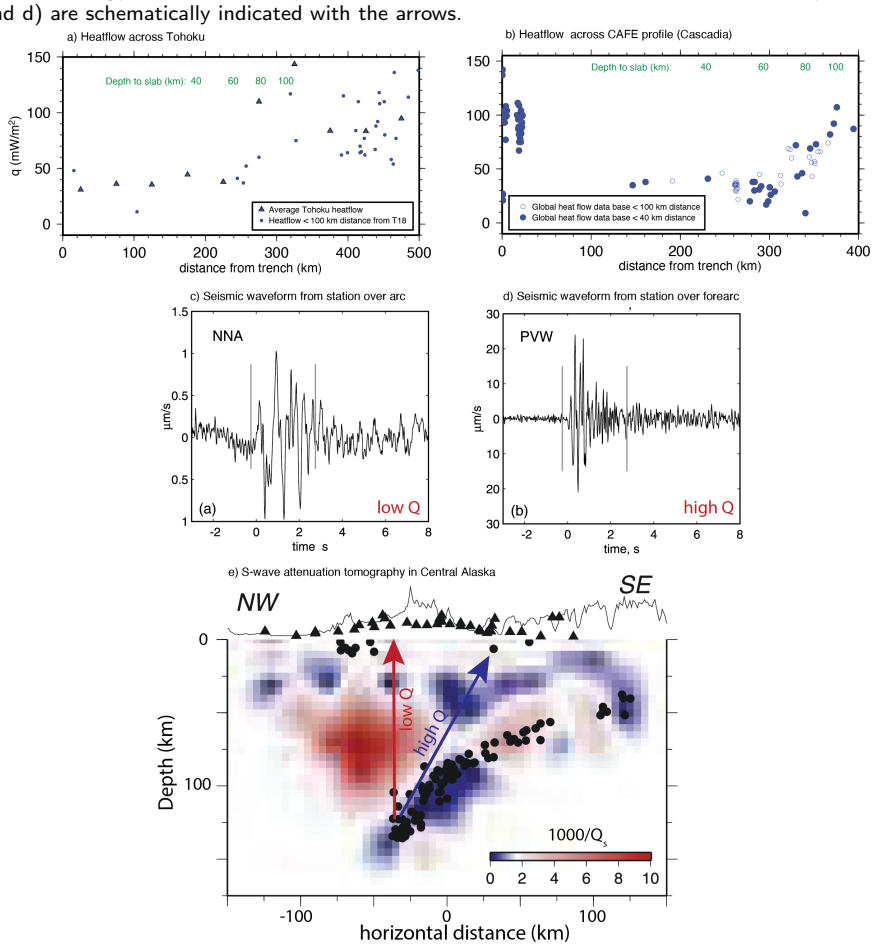

2.2 Seismology

Seismological methods provide critical information on the geometry of the subducting slab and structure of the overlying mantle wedge. For example, teleseismic determinations of intermediate-depth and deep seismicity in Wadati-Benioff zones have been used to delineate the position of subducting slabs (Gudmundsson and Sambridge, 1998). Important improvements over these early models include earthquake hypocenter relocation using global tomographic models (e.g., Portner and Hayes, 2018; Syracuse and Abers, 2006). Additional information can be obtained

from active-source seismic studies, local seismicity catalogs, and the use of PS and SP converted phases at velocity interfaces that may provide information about the location of the Moho or the top of the subducting crust (Bostock, 2013; Kim et al., 2021; Zhao et al., 1994). The most recent and comprehensive global slab surface geometries using a combination of these techniques is provided by Hayes et al. (2018). Local earthquake conversions (Shiina et al., 2013) and guided-wave studies (e.g., Abers et al., 2006; Rondenay et al., 2008) provide information on the hydration state of the subducting crust which can further constrain thermal models.

Observations of seismic attenuation (which is a measure of the absorption of seismic energy by non-elastic processes) is highly sensitive to temperature (Faul and Jackson, 2005; Takei, 2017) and can be used to map out in particular the hot regions in subduction zones. Commonly observed features are a low attenuation slab dipping below a high attenuation mantle wedge. Seismic attenuation is quantified by the quality factor Q which is inversely proportional to the degree of attenuation. It has been a common and long-standing observation (e.g., Sacks, 1968; Utsu, 1966) that waveforms from local earthquakes tend to have higher frequency and higher amplitude characteristics when they are observed by stations in the forearc compared to those observed in the arc and backarc (Figure 3c,d). In many regions it has now become possible to map out the attenuation structure in subduction zones in enough detail to see clear evidence of the cold corner with often a sharp, near-vertical boundary separating the nose of the wedge down to a slab depth of 75–80 km from the strongly attenuating mantle wedge below the arc and back-arc. Such regions include Peru (Jang et al., 2019), New Zealand (Eberhart-Phillips et al., 2020), the Lesser Antilles (Hicks et al., 2023), Tohoku (Nakajima et al., 2013), Nicaragua (Rychert et al., 2008), Central Alaska (Stachnik et al., 2004, Figure 3e), Ryukyu (Ko et al., 2012), the Aegean (Ventouzi et al., 2018), Tonga (Wei and Wiens, 2018), and the Marianas (Pozgay et al., 2009). In contrast, a 3D attenuation study of the Kyushu subduction zone showed low Q in the forearc mantle (Saita et al., 2015) which the authors contributed to a relatively high degree of serpentinization.

A weak and partially inverted Moho in Cascadia (Bostock et al., 2002; Brocher et al., 2003; Hansen et al., 2016) further illustrates the unusual nature of the forearc mantle. The crust-mantle interface is generally seen as a strong velocity contrast with a change from low crustal velocities to higher mantle velocities. This is the case in the backarc of Cascadia, but the near disappearance of the Moho and partial inversion below the forearc here suggests that the underlying mantle wedge has a lower seismic velocity than the ambient mantle. Extensive serpentinization has been suggested as main cause for this velocity change (Bostock et al., 2002) but the change could also be due to the gabbroic nature of the overlying Siletzia terrain (Crosbie et al., 2019). Low V_p velocities in the cold corner seem to be largely limited to Cascadia (Abers et al., 2017). This is likely due to the less efficient dehydration of the slab (and limited sourcing of fluids to the overlying forearc mantle wedge) in most other, colder, subduction zones (van Keken et al., 2011).

Of further note, particularly for subduction zones in northeastern Japan and Ryukyu, is a marked transition in SKS splitting between forearc and arc (e.g., Long and van der Hilst, 2005; Nakajima and Hasegawa, 2004). This has been interpreted by some to represent B-type olivine fabric in the cold, moderately hydrated, and

relatively high-stress cold corner (Kneller et al., 2007; Long and van der Hilst, 2006). It could alternatively be due to the crystal-preferred orientation formed by deformation of serpentine (e.g., Brownlee et al., 2013; Horn et al., 2020; Katayama et al., 2009; Mookherjee and Capitani, 2011; Nagaya et al., 2016; Wang et al., 2019) or perhaps is caused by a combination of these two mechanisms (Kneller et al., 2008; McCormack et al., 2013). Wang et al. (2019) also demonstrated clear evidence of the slab-mantle decoupling depth from anisotropic imaging. Of note here is the anisotropy observed from SKS splitting in Central Alaska, with a marked shift in direction of splitting, but now from trench-normal in the forearc and trench-parallel in the arc and backarc region (Christensen and Abers, 2010). It should be noted that the idea of slow convection with weak fabric development in the forearc of the northeastern Japan subduction zone may need revision given new off-shore seismic evidence that the forearc here may be stagnant and that the weak trench-parallel anisotropy originates from pre-existing fabric in the subducting crust (Uchide et al., 2020).

2.3 Geodetics

An intriguing new approach to physically map the extent and properties of the cold corner is through the use of postseismic deformation following large seismic events. Forward modeling can be used to constrain the differences in rheological behavior between a mostly elastic forearc mantle compared to the visco-plastic arc and backarc. This became a focus in modeling studies of the aftermath of the Tohoku-oki earthquake that took into account the properties of the Pacific slab. Such models require a thermal structure with a cold forearc separated from a warm arc region similar to that suggested from heat flow and seismology as described above (Freed et al., 2017; Hu et al., 2014; Luo and Wang, 2021; Muto et al., 2016, 2019). A useful review of this evolution in thought is in Dhar et al. (2023). Alternative models that focused primarily on temperature-dependent rheology also require a similar thermal structure to fit postseismic uplift data (e.g., Peña et al., 2020; van Dinther et al., 2019). Dhar et al. (2022) used a newly deployed geodetic network to demonstrate along-arc variations in the structure of the cold nose, with a narrowing of the nose below Miyagi and a broadening below Fukushima.

2.4 The cold corner requires mechanical decoupling between the slab and shallow mantle wedge

The geophysical evidence presented above requires the presence of a cold corner in the mantle wedge. This in itself requires that this part of the wedge is mostly isolated from the convective cornerflow and that therefore the slab remains decoupled below the seismogenic zone to a depth of 75–80 km. The geophysical data also require a relatively sharp transition to full slab-wedge coupling below this depth. In Figure 4 we reevaluate the classical models by Furukawa (1993) for the Cascadia subduction zone. The model is similar to the Cascadia model in Syracuse et al. (2010) but has been modified for the geometry, convergence velocity, and age at the trench of the slab below the imaging Magma Under mount St. Helens (iMUSH) array (Mann et al., 2019). In this model we also take into account the low radiogenic heat production in the continental crust due to the gabbroic nature of the accreted

Figure 4 Demonstration that heat flow constraints show that the slab should remain decoupled from the overriding mantle wedge well past the Moho. In all frames T indicates the location of the trench and VF that of the volcanic front. a) Figure redrawn from Furukawa (1993) (faithfully reproduced with the missing horizontal scale). Solid lines: heat flow predicted from his models with a decoupling depth increasing from 40 to 100 km. Gray boxes: averages of the available heat flow data at the time. b) Heat flow data for Cascadia with heat predictions from a model below the iMUSH profile over Mount St. Helens and Mount Adams (see text) with the same decoupling depths as in Furukawa (1993) in addition to d_c=80 km that we use in most of our subduction zone models. Open and filled blue circles as in Figure 3b but now with the global heat flow database entries projected onto the iMUSH profile. Small grey triangles are the BSR-derived data from Salmi et al. (2017) projected onto the iMUSH profile. c)-e): 2D temperature plots for the iMUSH cross sections with decoupling depth ranging from 40 km (c), to 70 km (d), and 100 km (e). The volcanic front is taken to be the location of Mount Adams. While the heat flow data would allow a 100 km decoupling depth the location of the volcanic front clearly does not.

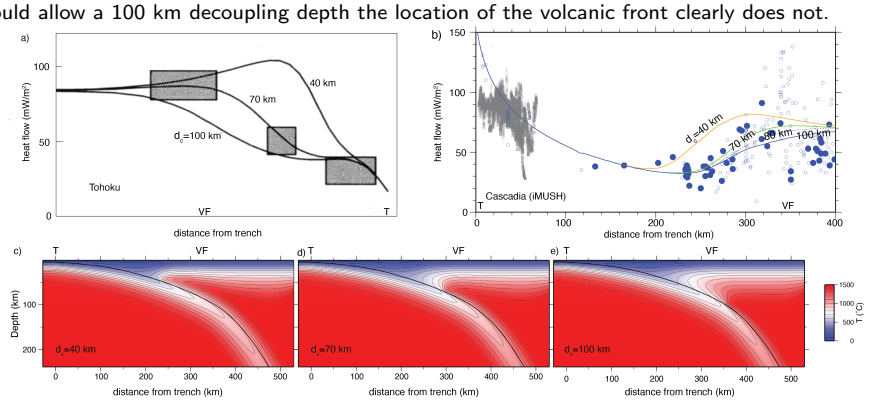

Siletzia terrane (Wells et al., 2014), which explains the very low heat flow in the forearc region (Figure 4b). The models are more fully described in Pang et al. (2023) and are available in the Supplementary Information (see data availability statement). These models show that heat flow and position of the volcanic arc are not satisfied by a very shallow (40 km) or deep (100 km) decoupling point, but that a depth of around 70–80 km gives satisfactory model results. Other examples are in Wada and Wang (2009).

We will not delve deeply into the very interesting question of why this decoupling seems to end at that depth but one can find abundant interest and suggestions for potential causes in the literature. Proposed mechanisms and features include the presence of weak phases such as serpentinite (Burdette and Hirth, 2022; Wada et al., 2008), the role of secondary phases (Peacock and Wang, 2021), or the convolution of multiple competing effects (Kerswell et al., 2021). It should be noted that explanations that rely on dehydration reactions that are largely isothermal at 2–4 GPa (such as those of antigorite and chlorite) lead to dynamics that are difficult to reconcile with a fixed-depth transition (see, e.g., the T550 models in Syracuse et al., 2010). Note also that the weak nature of antigorite has been recently questioned using experiments that showed stronger, semi-brittle deformation under relevant forearc conditions (Hirauchi et al., 2020).

We will in the remainder of this pair of papers assume that the slab is decoupled from the overriding crust and mantle to a depth of 80 km at which point it couples to and drags down the overriding mantle wedge (Figure 1). We will then explore the resulting effects on the thermal field in subduction zones and compare these to observations.

3 Selected literature examples of numerical models exploring subduction zone thermal structure

In wrapping up part I of this review paper we will highlight a few modeling studies. The literature covering approaches to understand and use the thermal structure of subduction zones through modeling is vast and cannot be covered fully in an introductory review. To limit our present scope we will focus on literature that was published in the last decade or so and that studies the thermal structure of the Japanese subduction systems in particular.

3.1 Why Japan?

Subduction zones in Japan (Figure 5a) are predicted to have a broad range of thermal structure with the thermal parameter ranging across more than an order of magnitude, from the relatively slow subduction of the young Philippine Sea Plate in Nankai (thermal parameter Φ=450 km) to fast subduction of old oceanic lithosphere in NE Japan (Φ=5100–6000 km), with intermediate conditions for Ryukyu and Kyushu (Φ=1600–2100 km). An introductory tour of thermal models of this region will therefore provide us with an efficient and focused way of exploring the features that may characterize the global subduction system.

3.2 Nankai

The shallow structure of the Nankai subduction zone is of particular interest to understand the mechanisms leading to large underthrusting events and the role of low frequency earthquakes, tectonic tremors, and slow slip. Harris et al. (2013) complemented a synthesis of the extensive off-shore heat flow measurements with 2D thermal modeling to show that heat flow data suggest pervasive fluid flow in the oceanic crust. This leads to differences in estimates of temperature along the seismogenic zone of up to 100°C compared to models that do not take this fluid flow into account. Hamamoto et al. (2011) also combined heat flow data and 2D thermal modeling to show that the shear stress on the plate interface in the central part of the Nankai Trough is very low. Using the, at the time, most recent heat flow data, Yoshioka et al. (2013) demonstrated, using thermal models along a number of 2D cross sections, the importance of shear heating along the plate interface and that the thermal effects of surface erosion and sedimentation due to Quaternary deformation has to be taken into account. Suenaga et al. (2019) performed 2D thermal modeling to show that the metamorphic phase change from amphibolite to eclogite with its associated fluid release controls the location of low-frequency earthquakes and tectonic tremors.

A combination of features makes the Nankai subduction zone very challenging for thermal modeling. These include: relative recent (re)initiation of subduction of the Philippine Sea Plate into a region of mature subduction of the Pacific below NW Japan; the complicated and time-variable tectonic history (Kimura et al., 2005); the variable age of the incoming lithosphere (e.g., Seno and Maruyama, 1984); and changes in apparent dip along-strike (see discussion in Wang et al., 2004). In addition, the proximity of the Euler pole between the Philippine Sea Plate and the Eurasian plate (Seno, 1977) causes oblique convergence with changes of obliquity along strike. This suggests that we can draw the most confidence from models

Figure 5 a) Map of the Japanese subduction systems. Black contours show depth to the top of the subducting slab (from Hayes et al., 2018) for the Japan, Nankai, Kyushu, and Ryukyu segments at 10 km intervals (50 km intervals are in bold). Red triangles show locations of arc volcanoes. Orange lines are plate boundaries from Bird (2003). Age of oceanic lithosphere is from Müller et al. (2008). b) 3D model showing subduction of the Philippine Sea Plate (PHS) and Pacific slab below the Kanto region (modified from Wada and He, 2017). MDD=maximum decoupling depth (denoted as d_c in this paper). c) Heat flow comparison between observations (Tanaka et al., 2004) and model predictions (also modified from Wada and He, 2017). d) Predicted "blueschist-out" boundary below Tohoku (modified from Morishige, 2022) assuming this occurs, as in van Keken et al. (2012), at T=617−52P (in °C with P in GPa). Compare with Figure 2b. e) as frame d) but now for the serpentinite-out boundary using, as in Faccenda et al. (2012), T=740−1.8P−3.9P^2 at $P\geq$2.1 GPa and T=478+180P−31P^2 at $P\leq$2.1 GPa.

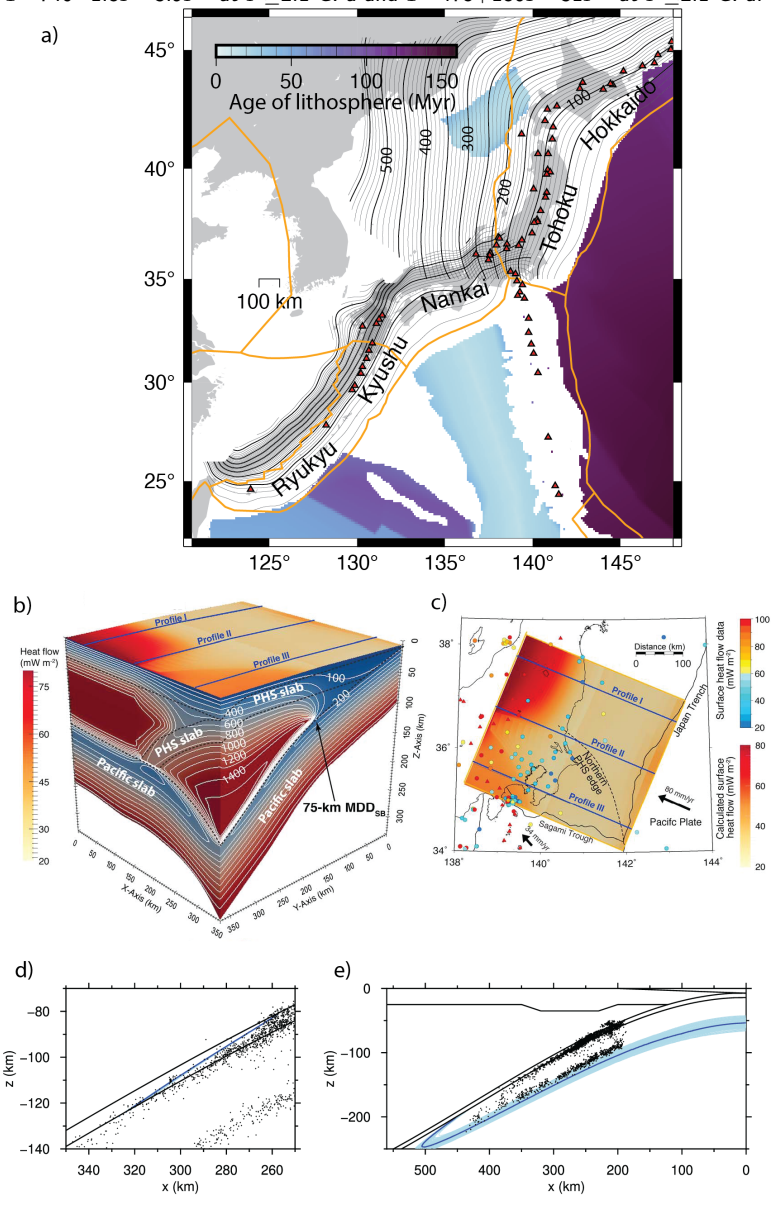

that are 3D, time-dependent, and take time-dependent changes in the age of the

incoming slab and convergence parameters into account. Such studies are, aside from complicated, quite expensive computationally but there are a few such studies that we can highlight. Ji et al. (2016) showed that the changes in obliquity caused significant variations in temperature along the plate interface providing a potential example for lateral changes in the occurrence of low-frequency earthquakes and slow slip events. Morishige and van Keken (2017) focused on changes in curvature of the slab and suggested that focused fluid migration explains along-strike differences in accumulated slip rates of slow slip events. Wada and He (2017) focused on the interaction between the recently subducting Philippine Sea plate into the mature subducting of the Pacific below the Kanto region (Figure 5b). This study confirmed that the heat flow data were best explained by a decoupling depth of 75 km here (Figure 5c). Given the relatively young age of the Nankai subduction zone this study suggests the characteristics of the plate interface that lead to the cold corner establishes early. They also found that the down-dip limit of the seismogenic zone is characterized by the 350°C isotherm throughout the region.

3.3 Tohoku and Hokkaido

For a thermal modeler, the relatively uniform subduction of the old Pacific lithosphere below NW Japan provides a welcome respite from the complications in Nankai. Convergence becomes somewhat oblique when moving north from the Japan Trench to the Kurile Trench but convergence characteristics vary relatively little along strike.

Extending the suggestion by Kita et al. (2010b), van Keken et al. (2012) demonstrated that the uppermost seismicity contained within ∼7 km from the slab top is controlled by metamorphic dehydration reactions in the subducting oceanic crust by showing that, to reasonable confidence, this seismicity disappears at the blueschist-out dehydration reaction across most of the Tohoku-Hokkaido subduction zone. An important exception was for a cross-section across SW Hokkaido. Below this region the seismic belt deepens anomalously which was suggested to be caused by the thermal effects of subducted forearc crust (Kita et al., 2010a). Using 2D modeling, van Keken et al. (2012) failed to confirm this hypothesis and suggested that 3D flow caused by geometrical changes at the junction of the Tohoku-Kurile arc (as demonstrated by Morishige and Honda, 2013) may be the real cause for the anomalous characteristics of upper plane seismicity here. Using 3D thermal modeling Morishige and van Keken (2014) provided a negative test of this hypothesis. They showed that the thermal variations caused by 3D flow were too small to explain the deepening of the seismic belt. By contrast, Wada et al. (2015) were able to show a significant cooling of the mantle wedge at the transition between the Tohoku and Hokkaido subduction zones potentially because they used a more realistic slab geometry than the idealized one in Morishige and van Keken (2014). Wada et al. (2015) also cautioned that the cooling effect they predicted might be an overestimate due to the assumption of steady state. This suggests that the anomalous character of subduction below SW Hokkaido remains an important topic for future research.

The Tohoku subduction zone was the focus in a study by Morishige (2022) to test whether variable thermal properties (such as thermal conductivity and thermal

expansivity) could have a significant effect on the thermal structure of the subducting slab. A novel aspect of this study was the use of a Bayesian inversion to make sure the thermal structure of the incoming plate satisfied constraints from heat flow and bathymetry. The conclusion of this study was that one could use constant thermal properties since differences in thermal structure between these two assumptions were found to be small. It confirmed the importance of the blueschist-out boundary on controlling the depth of the upper belt of seismicity (Figure 5d) and showed that the lower plane of the double seismic zone was in the serpentinite stability field (Figure 5e), confirming earlier suggestions that the deeper plane seismicity might be related to the production of fluids by metamorphic dehydration of the slab mantle (e.g., Faccenda et al., 2012; Hacker et al., 2003; Peacock, 2001).

Horiuchi and Iwamori (2016) explored fluid release and flow in the mantle wedge below Tohoku. They showed they could to a reasonable degree match observations of the location of the volcanic arc, seismic tomography, and heat flow if the initial water content of the incoming slab was 2–3 wt% and the viscosity of the modeled serpentinite layer was in the range of 10^{20}–10^{21} Pa·s. Yoo and Lee (2023) provided a similar study of fluid production and release along with melt generation and freezing. They suggested that the observed melt focusing below the Tohoku volcanic arc can be best explained by a relatively deep decoupling depth (90 km) with an important role for melt freezing.

3.4 Kyushu and Ryukyu

The Kyushu and Ryukyu subduction zones are characterized by faster (∼7 cm/yr), more mature, and steeper subduction of somewhat older (27–43 Myr) lithosphere compared to Nankai. These subduction zones have a northern termination at the Kyushu-Palau ridge and end to the south at Taiwan.

There are a few studies of note in this region that particularly focused on constraining thermal conditions from the seismic characteristics of the plate interface. Thermal modeling showed that lateral variations in the characteristics of short-term slow slip events in Ryukyu could not be explained by thermal variations alone, but could be due to variable fluid flux from the oceanic crust (Suenaga et al., 2021). Gutscher et al. (2016) used 2D thermal models near the southern termination of the Ryukyu subduction zone combined with the characteristics of the seismogenic zone to argue either for a thermal rejuvenation of the westernmost Philippine Sea Plate or that toroidal flow in the mantle wedge caused warmer than expected conditions here (see also the discussion in part II about 3D flow effects on thermal structure). Using a 2D model for Kyushu that matched local heat flow data, Suenaga et al. (2018) showed that tectonic tremors occurred in the mantle wedge corner at temperatures between 450–650°C and that the afterslip of the 1996 Hyuga-nada earthquake occurred where the plate interface is at 300–350°C. This is at the high end of temperatures suggested for the seismogenic zone (Hyndman et al., 1995) suggesting therefore that maximum afterslip occurred near the down-dip end of the seismogenic zone in their model.

4 Conclusions for Part I

We provided the motivation for the need to understand the thermal structure through geodynamical modeling and provided a select number of examples of such

models. In part II we will turn to explore numerical methods that can be used to model this thermal structure, provide ways to test the quality of such models, and provide a comparison between model predictions for subduction zone temperatures and observations of these from geochemical and geophysical observations.

Availability of data and material

All geophysical and geochemical data and all modeling studies presented (except those in frames b through e of Figure 4) are taken from the literature. Modelled temperature and heat flow for Figure 4 (frames b through e) are available via the Zenodo repository doi.org/10.5281/zenodo.7843967.

Competing interests

The authors declare that they have no competing interest.

Funding

No funding was obtained for this study.

Authors' contributions

Both authors conceived of the approach to the review paper. Both authors contributed to writing this paper.

Acknowledgements

PvK thanks the JpGU for providing travel funding to the most recent pre-COVID and in-person JpGU-AGU meeting in Chiba, Japan. We thank Geoff Abers, Sambuddha Dhar, and two anonymous reviewers for their comments on and suggestions for an earlier version of the manuscript. This allowed us to improve the general flow of the manuscript, the quality of the figures, and in particular the seismological and geodetic descriptions. We also thank Geoff Abers for providing the heat flow data along the iMUSH profile in Figure 4b.

Endnotes

References

Abers, G.A, van Keken, P.E, Hacker, B.R (2017) The cold and relatively dry nature of mantle forearcs in subduction zones. Nat Geosc 10, 333–337. doi:10.1038/ngeo2922

Abers, G.A, van Keken, P.E, Kneller, E.A, Ferris, A, Stachnik, J.C (2006) The thermal structure of subduction zones constrained by seismic imaging: Implications for slab dehydration and wedge flow. Earth Planet Sci Lett 241, 387–397. doi:10.1016/j.epsl.2005.11.055

Abers, G.A, MacKenzie, L.S, Rondenay, S, Zhang, Z, Wech, A.G, Creager, K.C (2009) Imaging the source region of Cascadia tremor and intermediate-depth earthquakes. Geology 37, 1119–1122. doi:10.1130/G30143A.1

Abers, G.A, Nakajima, J, van Keken, P.E, Kita, S, Hacker, B.R (2013) Thermal-petrological controls on the location of earthquakes within subducting plates. Earth Planet Sci Lett 369–370, 178–187. doi:10.1016/j.epsl.2013.03.022

Agata, R, Barbot, S.D, Fujita, K, Hyodo, M, Iinuma, T, Nakata, R, Ichimura, T, Hori, T (2019) Rapid mantle flow with power-law creep explains deformation after the 2011 Tohoku mega-quake. Nat Comm **10**. Art No 1385, doi:10.1038/s41467-019-0984-7

Arzilli, F, Burton, M, La Spina, G, Macpherson, C.G, van Keken, P.E, McCann, J (2023) Decarbonation of subducting carbonate-bearing sediments and basalts of altered oceanic crust: Insights into recycling of CO_2 through volcanic arcs. Earth Planet Sci Lett **602**. Art No 117945, doi:10.1016/j.epsl.2022.117945

Bang, Y, Hwang, H, Kim, T, Cynn, H, Park, Y, Jung, H, Park, C, Popov, D, Prakapenka, V.B, Wang, L, Liermann, H-P, Irifune, T, Mao, H-K, Lee, Y (2021) The stability of subducted glaucophane with the Earth's secular cooling. Nat Comm **12**. Art No 1496, doi:10.1039/s41467-021-21746-8

Bebout, G.E, Penniston-Dorland, S.C (2016) Fluid and mass transfer at subduction interfaces – The field metamorphic record. Lithos 240–243, 228–258. doi:10.1016/j.lithos.2015.10.007

Bellot, N, Boyet, M, Doucelance, R, Bonnand, P, Savov, I.P, Plank, T, Elliott, T (2018) Origin of negative cerium anomalies in subduction-related volcanic samples: Constraints from Ce and Nd isotopes. Chem Geo 500, 46–63. doi:10.1016/j.chemgeo.2018.09.006

Bird, P (2003) An updated digital model of plate boundaries. Geochem Geophys Geosys **4**. Art No 1027, doi:10.1029/2001GC000252

Bloch, W, John, T, Kummerow, J, Salazar, P, Krüger, O, Shapiro, S (2018) Watching dehydration: Seismic indication for transient fluid pathways in the oceanic mantle of the subducting Nazca slab. Geochem Geophys Geosys 19, 3189–3207. doi:10.1029/2018GC007703

Bostock, M.G (2013) The Moho in subduction zones. Tectonophysics 609, 547–557. doi:10.1016/j.tecto.2012.07.007

Bostock, M.G, Hyndman, R.D, Rondenay, S, Peacock, S.M (2002) An inverted continental Moho and serpentinization of the forearc mantle. Nature 417, 536–538. doi:10.1038/417536a

Brey, G.P, Girnis, A.V, Bulatov, V.K, Höfer, H.E, Gerdes, A, Woodland, A.B (2015) Reduced sediment melting at 7.5–12 GPa: phase relations, geochemical signals and diamond nucleation. Contrib Min Petrol **170**. Art No 18, doi:10.1007/s00410-015-1166-z

Brocher, T.M, Parsons, T, Tréhu, A, Snelson, C.M, Fisher, M.A (2003) Seismic evidence for widespread serpentinized forearc upper mantle along the Cascadia margin. Geology 31, 267–270. doi:10.1130/0091-7613(2003)031<0267:SEFWSF>2.0CO;2

Brownlee, S.J, Hacker, B.R, Harlow, G.E, Seward, G (2013) Seismic signatures of a hydrated mantle wedge from antigorite crystal-preferred orientation (CPO). Earth Planet Sci Lett 375, 395–407. doi:10.1016/j.epsl.2013.06.003

Burdette, E, Hirth, G (2022) Creep rheology of antigorite: Experiments at subduction zone conditions. J Geophys Res: Solid Earth **127**. Art No e2022JG024260, doi:10.1029/2022JB024260

Cannaò, E, Tiepolo, M, Bebout, G.E, Scambelluri, M (2020) Into the deep and beyond: Carbon and nitrogen subduction recycling in secondary peridotites. Earth Planet Sci Lett **543**. Art No 116328, doi:10.1016/j.epsl.2020.116328

Cedeño, D.G, Conceição, R.V, Souza, M.R.W, Quinteiro, R.V.C, Carniel, L.C, Ketzer, J.M.M, Rodrigues, F, Bruzza, E.C (2019) An experimental study on smectites as nitrogen conveyors in subduction zones. Appl Clay Sci 168, 409–420. doi:10.1016/j.clay.2018.11.006

Chen, S, Guo, X, Yoshino, T, Jin, Z, Li, P (2018) Dehydration of phengite inferred by electrical conductivity measurements: Implications for the high conductivity anomalies relevant to the subduction zones. Geology 46, 11–14. doi:10.1130/G39716

Christensen, D.H, Abers, G.A (2010) Seismic anisotropy under central Alaska from SKS splitting observations. J Geophys Res: Solid Earth **115**. Art No B04315, doi:10.1029/2009JB006712

Christeson, G.L, Goff, J.A, Reece, R.S (2019) Synthesis of oceanic crustal structure from two-dimensional seismic profiles. Rev Geophys 57, 504–529. doi:10.1029/2019RG000641

Codillo, E.A, Klein, F, Marschall, H.R (2022) Preferential formation of chlorite over talc during Si-metasomatism of ultramafic rocks in subduction zones. Geophys Res Lett **49**. Art No e2022GL100218, doi:10.1029/2022GL100218

Condit, C.B, Guevara, V.E, Delph, J.R, French, M.E (2020) Slab dehydration in warm subduction zones at depths of episodic slip and tremor. Earth Planet Sci Lett **552**. Art No 116601, doi:10.1016/j.epsl.2020.116601

Crosbie, K.J, Abers, G.A, Mann, M.E, Janiszewski, H.A, Creager, K.C, Ulberg, C.W, Moran, S.C (2019) Shear velocity structure from ambient noise and teleseismic surface wave tomography in the Cascades around Mount St. Helens. J Geophys Res: Solid Earth 124, 8358–8375. doi:10.1029/2019JB017836

Currie, C.A, Wang, K, Hyndman, R.D, He, J (2004) The thermal effects of steady-state slab-driven mantle flow above a subducting plate: the Cascadia subduction zone and backarc. Earth Planet Sci Lett 223, 35–48. doi:10.1016/j.epsl.2004.04.020

Dhar, S, Muto, J, Ito, Y, Miura, S, Moore, J.D.P, Ohta, Y, Iinuma, T (2022) Along-arc heterogeneous rheology inferred from post-seismic deformation of the 2011 Tohoku-oki earthquake. Geophys J Int 230, 202–215. doi:10.1093/gji/ggac063

Dhar, S, Muto, J, Ohta, Y, Iinuma, T (2023) Heterogeneous rheology of Japan subduction zone revealed by postseismic deformation of the 2011 Tohoku-oki earthquake. Prog Earth Planet Sci **10**. Art No 9 (2023), doi:10.1186/s40645-023-00539-1

Eberhart-Phillips, D, Bannister, S, Reyners, M (2020) Attenuation in the mantle wedge beneath super-volcanoes of the Taupo Volcanic Zone, New Zealand. Geophys J Int 220, 703–723. doi:10.1093/gji/ggz455

Faccenda, M, Gerya, T.V, Mancktelow, N.S, Moresi, L (2012) Fluid flow during slab unbending and dehydration: Implications for intermediate-depth seismicity, slab weakening and deep water recycling. Geochem Geophys Geosys **13**. Art No Q01010, doi:10.1029/2011GC003860

Fagereng, Å, Diener, J.F.A, Ellis, S, Remitti, F (2018) Fluid-related deformation processes at the up- and downdip limit of the subduction thrust seismogenic zone: What do the rocks tell us? In: Byrne, T, Underwood III, M.B, Fisher, D, McNeill, L, Saffer, D, Ujiie, K, Yamaguchi, A (eds.) Geology and Tectonics of Subduction Zones: A Tribute to Gaku Kimura. GSA Special Publication 534. Geological Society of America, Boulder, CO, USA. doi:10.1130/SPE534

Farsang, S, Louvel, M, Zhao, C, Mezouar, M, Rosa, A.D, Widmer, R.N, Feng, X, Liu, J, Redfern, S.A.T (2021) Deep carbon cycle constrained by carbonate solubility. Nat Comm **12**. Art No 4311, doi:10.1038/s41467-021-24533-7

Faul, U.H, Jackson, I (2005) The seismological signature of temperature and grain size variations in the upper mantle. Earth Planet Sci Lett 234, 119–134. doi:10.1016/j.epsl.2005.02.008

Ferrand, T.P (2019) Seismicity and mineral destabilizations in the subducting mantle up to 6 GPa, 200 km depth. Lithos 334–335, 205–230. doi:10.1016/j.lithos.2019.03.014

Fisher, D.M, Smye, A.J, Marone, C, van Keken, P.E, Yamaguchi, A (2019) Kinematic models for healing of the subduction interface based on observations of ancient accretionary complexes. Geochem Geophys Geosys 20, 3431–3449. doi:10.1029/2019GC008256

Förster, M.W, Selway, K (2021) Melting of subducted sediments reconciles geophysical images of subduction zones. Nat Comm **12**. Art No 1320, doi:10.1038/s41467-021-21657-8

Freed, A.M, Hashima, A, Becker, T.W, Okaya, D, Sato, H, Hatanaka, Y (2017) Resolving depth-dependent subduction zone viscosity and afterslip from postseismic displacements following the 2011 Tohoku-oki, Japan earthquake. Earth Planet Sci Lett 456, 279–290. doi:10.1016/j.epsl.2016.11.040

Frohlich, C (2006) Deep Earthquakes. Cambridge University Press, Cambridge, UK. doi:10.1017/CB09781107297562

Furukawa, Y (1993) Depth of the decoupling plate interface and thermal structure under arcs. J Geophys Res: Solid Earth 98, 20005–20013. doi:10.1029/93JB02020

Furukawa, Y, Uyeda, S (1989) Thermal state under the Tohoku arc with consideration of crustal heat generation. Tectonophysics 164, 175–187. doi:10.1016/0040-1951(89)90011-5

Gudmundsson, Ó, Sambridge, M (1998) A regional upper mantle (RUM) seismic model. J Geophys Res: Solid Earth 103, 7121–7136. doi:10.1029/97JB02488

Guo, H, Keppler, H (2019) Electrical conductivity of NaCl-bearing aqueous fluids to 900°C and 5 GPa. J Geophys Res: Solid Earth 124, 1397–1411. doi:10.1029/2018JB016658

Gutscher, M-A, Klingelhoefer, F, Theunissen, T, Spakman, W, Berthet, T, Wang, T.K, Lee, C-S (2016) Thermal modeling of the SW Ryukyu forearc (Taiwan): Implications for the seismogenic zone and the age of the subducting Philippine Sea Plate (Huatung Basin). Tectonophysics 692, 131–142. doi:10.1016/j.tecto.2016.03.029

Hacker, B.R (2008) H_2O subduction beyond arcs. Geochem Geophys Geosys **9**. Art No Q03001,

740 doi:10.1029/2007GC001707
741 Hacker, B.R, Peacock, S.M, Abers, G.A, Holloway, S.D (2003) Subduction factory 2. Are intermediate-depth
742 earthquakes in subducting slabs linked to metamorphic dehydration reactions? J Geophys Res: Solid Earth
743 **108**. Art No 2030, doi:10.1029/2001JB001129
744 Hamamoto, H, Yamano, M, Goto, S, Kinoshita, M, Fujino, K, Wang, K (2011) Heat flow distribution and thermal
745 structure of the Nankai subduction zone off the Kii Peninsula. Geochem Geophys Geosys **12**. Art No
746 Q0AD20, doi:10.1029/2011GC003623
747 Hansen, S.M, Schmandt, B, Levander, A, Kiser, E, Vidale, J.E, Abers, G.A, Creager, K.C (2016) Seismic evidence
748 for a cold serpentinized mantle wedge beneath Mount St Helens. Nat Comm **7**. Art No 13242,
749 doi:10.1038/ncoms13242
750 Harris, R.N, Grevemeyer, I, Ranero, C.R, Villinger, H, Backhausen, U, Henke, T, Mueller, C, Neben, S (2010)
751 Thermal regime of the Costa Rican convergent margin: 1. Along-strike variations in heat flow from probe
752 measurements and estimated from bottom-simulating reflectors. Geochem Geophys Geosys **11**. Art No
753 Q12S28, doi:10.1029/2010GC003272
754 Harris, R, Yamano, M, Kinoshita, M, Spinelli, G, Hadamoto, H, Ashi, J (2013) A synthesis of heat flow
755 determinations and thermal modeling along the Nankai Trough, Japan. J Geophys Res: Solid Earth 118,
756 2687–2702. doi:10.1002/jgrb.50230
757 Hayes, G.P, Moore, G.L, Portner, D.E, Flamme, H, Furtney, M, Smoczyk, G.M (2018) Slab 2, a comprehensive
758 subduction zone geometry model. Science 362, 58–61. doi:10.1126/science.aat4723
759 Henry, S.G, Pollack, H.N (1988) Terrestrial heat flow above the Andean subduction zone in Bolivia and Peru. J
760 Geophys Res: Solid Earth 93, 15153–15162. doi:10.1029/JB093iB12p15153
761 Henrys, S.A, Ellis, S, Uruski, C (2003) Conductive heat flow variations from bottom-simulating reflectors on the
762 Hikurangi margin, New Zealand. Geophys Res Lett **30**. Art No 1065, doi:10.1029/2002GL015772
763 Hermann, J, Lakey, S (2021) Water transfer to the deep mantle through hydrous, Al-rich silicates in subduction
764 zones. Geology 49, 911–915. doi:10.1130/G48658.1
765 Hernández-Uribe, D, Hernández-Montenegro, J.D, Cone, K.A, Palin, R.M (2019) Oceanic slab-top melting during
766 subduction: Implications for trace-element recycling and adakite petrogenesis. Geology 48, 216–220.
767 doi:10.1130/G46835.1
768 Hicks, S.P, Bie, L, Rychert, C.A, Harmon, N, Goes, S, Rietbrock, A, Wei, S.S, Collier, J, Henstock, T.J, Lynch, L,
769 Prytulak, J, MacPherson, C.G, Schlaphorst, D, Wilkinson, J.J, Blundy, J.D, Cooper, G.F, Davey, R.G,
770 Kendall, J-M, VoiLA Working Group (2023) Slab to back-arc to arc: Fluid and melt pathways through the
771 mantle wedge beneath the Lesser Antilles. Sci Adv **9**. Art No eadd2143, doi:10.1126/sciadv.add2143
772 Hirauchi, K-i, Katayama, I, Kouketsu, Y (2020) Semi-brittle deformation of antigorite serpentinite under forearc
773 mantle wedge conditions. J Struct Geol **140**. Art No 104151, doi:10.1016/j.jsg.2020.104151
774 Honda, S (1985) Thermal structure beneath Tohoku, northeast Japan – a case study for understanding the
775 detailed thermal structure of the subduction zone. Tectonophysics 112, 69–102.
776 doi:10.1016/0040-1951(85)90173-8
777 Horiuchi, S-s, Iwamori, H (2016) A consistent model for fluid distribution, viscosity distribution, and flow-thermal
778 structure in subduction zone. J Geophys Res: Solid Earth 121, 3238–3260. doi:10.1002/2015JB012384
779 Horn, C, Bouilhol, P, Skemer, P (2020) Serpentinization, deformation, and seismic anisotropy in the subduction
780 mantle wedge. Geochem Geophys Geosys **21**. Art No e2020GC008950, doi:10.1029/2020GC008950
781 Hu, H, Dai, L, Li, H, Hui, K, Sun, W (2017) Influence of dehydration on the electrical conductivity of epidote and
782 implications for high-conductivity anomalies in subduction zones. J Geophys Res: Solid Earth 122,
783 2751–2762. doi:10.1002/2016JB013767
784 Hu, Y, Teng, F-Z, Chauvel, C (2021) Potassium isotopic evidence for sedimentary input to the mantle source of
785 Lesser Antilles lavas. Geochim Cosmochim Acta 295, 91–111. doi:10.1016/j.gca.2020.12.013
786 Hu, Y, Teng, F-Z, Ionov, D.A (2020) Magnesium isotopic composition of metasomatized upper sub-arc mantle
787 and its implications to Mg cycling in subduction zones. Geochim Cosmochim Acta 278, 219–234.
788 doi:10.1016/j.gca.2019.09.030
789 Hu, Y, Bürgmann, R, Uchida, N, Banerjee, P, Freymueller, J.T (2014) Stress-driven relaxation of heterogeneous
790 upper mantle and time-dependent afterslip following the 2011 Tohoku earthquake. J Geophys Res: Solid
791 Earth 121, 385–411. doi:10.1002/2015JB012508
792 Huang, Y, Guo, H, Nakatani, T, Uesugi, K, Nakamura, M, Keppler, H (2021) Electrical conductivity in texturally
793 equilibrated fluid-bearing forsterite aggregates at 800°C and 1 GPa: Implications for the high electrical
794 conductivity anomalies in mantle wedges. J Geophys Res: Solid Earth **126**. Art No e2020JB021343,
795 doi:10.1029/2020JB021343
796 Hyndman, R.D, Davis, E.E, Wright, J.A (1979) The measurement of marine geothermal heat flow by a
797 multipenetration probe with digital acoustic telemetry and insitu thermal conductivity. Mar Geophys Res 4,
798 181–205. doi:10.1007/BF00286404
799 Hyndman, R.D, Wang, K, Yamano, M (1995) Thermal constraints on the seismogenic portion of southwestern
800 Japan subduction thrust. J Geophys Res: Solid Earth 100, 15373–15392. doi:10.1029/95JB00153
801 Hyndman, R.D, Foucher, J.P, Yamano, M, Fisher, A, Scientific Team of Ocean Drilling Program Leg 131 (1992)
802 Deep sea bottom-simulating reflectors: calibration of the base of the hydrate stability field as used for heat
803 flow estimates. Earth Planet Sci Lett 109, 289–301. doi:10.1016/0012-821X(92)90093-B
804 Jang, H, Kim, Y.H, Lim, H, Clayton, R.W (2019) Seismic attenuation structure of southern Peruvian subduction
805 system. Tectonophysics **771**. Art No 228203, doi:10.1016/j.tecto.2019.228203
806 Jégo, S, Dasgupta, J (2013) Fluid-present melting of sulfide-bearing ocean-crust: Experimental constraints on the
807 transport of sulfur from subducting slab to mantle wedge. Geochim Cosmochim Acta 110, 106–134.
808 doi:10.1016/j.gca.2013.02.011
809 Jégo, S, Dasgupta, J (2014) The fate of sulfur during fluid-present melting of subducting basaltic crust at variable
810 oxygen fugacity. J Petrol 55, 1019–1050. doi:10.1093/petrology/egu016
811 Ji, Y, Yoshioka, S, Matsumoto, T (2016) Three-dimensional numerical modeling of temperature and mantle flow

fields associated with subduction of the Philippine Sea plate, southwest Japan. J Geophys Res: Solid Earth 121, 4458–4482. doi:10.1002/2016JB012912

Jung, H, Green II, H.W, Dobrzhinetskaya, L.F (2004) Intermediate-depth earthquake faulting by dehydration embrittlement with negative volume change. Nature 428, 545–549. doi:10.1038/nature02412

Katayama, I, Hirauchi, K-i, Michibayashi, K, Ando, J-i (2009) Trench-parallel anisotropy produced by serpentinite deformation in the hydrated mantle wedge. Nature 461, 1114–1117. doi:10.1038/nature08513

Kelemen, P.B, Hirth, G (2007) A periodic shear-heating mechanism for intermediate-depth earthquakes in the mantle. Nature 446, 787–790. doi:10.1038/nature05717

Kerswell, B.C, Kohn, M.J, Gerya, T.V (2021) Backarc lithospheric thickness and serpentine stability control slab-mantle coupling depths in subduction zones. Geochem Geophys Geosys **22**. Art No e2022GC009304, doi:10.1029/2020GC009304

Kim, H.J, Kawakatsu, H, Akuhara, T, Shinohara, M, Shiobara, H, Sugioka, H, Takagi, R (2021) Receiver function imaging of the amphibious NE Japan subduction zone – Effects of low-velocity sediment layer. J Geophys Res: Solid Earth **126**. Art No e2021JB021918, doi:10.1029/2021JB021918

Kimura, J-I (2017) Modeling chemical geodynamics of subduction zones using the Arc Basalt Simulator version 5. Geosphere 13, 992–1025. doi:10.1130/GES01468.1

Kimura, J-I, Nakajima, J (2014) Behaviour of subducted water and its role in magma genesis in the NE Japan arc: A combined geophysical and geochemical approach. Geochim Cosmochim Acta 143, 165–188. doi:10.1016/j.gca.2014.04.019

Kimura, J-I, Stern, R.J, Yoshida, T (2005) Reinitiation of subduction and magmatic responses in SW Japan during Neogene time. GSA Bull 117, 969–986. doi:10.1130/B25565.1

Kimura, J-I, Hacker, B.R, van Keken, P.E, Kawabata, H, Yoshida, T, Stern, R.J (2009) Arc Basalt Simulator version 2, a simulation for slab dehydration and fluid-flux mantle melting for arc basalts: Modeling scheme and application. Geochem Geophys Geosys **10**. Art No Q09004, doi:10.1029/2008GC002217

Kimura, J-I, Kent, A.J.R, Rowe, M, Katakuse, M, Nakano, F, Hacker, B.R, van Keken, P.E, Kawabata, H, Stern, R.J (2010) Origin of cross-chain geochemical variation in Quaternary lavas from the northern Izu arc: Using a quantitative mass balance approach to identify mantle sources and wedge processes. Geochem Geophys Geosys **11**. Art No Q10011, doi:10.1029/2010GC003050

Kimura, J-I, Gill, J.B, Kunikiyo, T, Osaka, I, Shimoshiori, Y, Katakuse, M, Kakabuchi, S, Nagao, T, Furuyama, K, Kamei, A, Kawabata, H, Nakajima, J, van Keken, P.E, Stern, R.J (2014) Diverse magmatic effects of subducting a hot slab in SW Japan: Results from forward modeling. Geochem Geophys Geosys 15, 691–739. doi:10.1002/2013GC005132

Kimura, J-I, Gill, J.B, Skora, S, van Keken, P.E, Kawabata, H (2016) Origin of geochemical mantle components: Role of subduction filter. Geochem Geophys Geosys 17, 3289–3325. doi:10.1002/2016GC006343

Kirby, S, Engdahl, E.R, Denlinger, R (1996) Intermediate-depth intraslab earthquakes and arc volcanism as physical expressions of crustal and uppermost mantle metamorphism in subducting slabs. In: Bebout, G.E, Scholl, D.W, Kirby, S.H, Platt, J.P (eds.) Subduction: Top to Bottom, Geophysical Monograph 96. American Geophysical Union, Washington, DC, USA, pp 195–214. doi:10.1029/GM096

Kita, S, Okada, T, Hasegawa, A, Nakajima, J, Matsuzawa, T (2010a) Anomalous deepening of a seismic belt in the upper-plane of the double seismic zone in the Pacific slab beneath the Hokkaido corner: Possible evidence for thermal shielding caused by subducted forearc crust materials. Earth Planet Sci Lett 290, 415–426. doi:10.1016/j.epsl.2009.12.038

Kita, S, Okada, T, Hasegawa, A, Nakajima, J, Matsuzawa (2010b) Existence of interplane earthquakes and neutral stress boundary between the upper and lower planes of the double seismic zone beneath Tohoku and Hokkaido, northeastern Japan. Tectonophysics 496, 68–82. doi:10.1016/j.tecto.2010.10.010

Kneller, E.A, Long, M.D, van Keken, P.E (2008) Olivine fabric transitions and shear wave anisotropy in the Ryukyu subduction system. Earth Planet Sci Lett 268, 268–282. doi:10.1016/j.epsl.2008.01.004

Kneller, E.A, van Keken, P.E, Katayama, I, Karato, S (2007) Stress, strain, and B-type olivine fabric in the fore-arc mantle: Sensitivity tests using high-resolution steady-state subduction zone models. J Geophys Res: Solid Earth **222**. Art No B04406, doi:10.1029/2006JB004544

Ko, Y-T, Kuo, B-Y, Wang, K-L, Lin, S-C, Hung, S-H (2012) The southwestern edge of the Ryukyu subduction zone: A high Q mantle wedge. Earth Planet Sci Lett 335–336, 145–153. doi:10.1016/j.epsl.2012.04.041

Lee, J, Mookherjee, M, Kim, T, Jung, H, Klemd, R (2021) Seismic anisotropy in subduction zones: Evaluating the role of chloritoid. Front Earth Sci **9**. Art No 644958, doi:10.3389/feart.2021.644958

Long, M.D, van der Hilst, R.D (2005) Upper mantle anisotropy beneath Japan from shear wave splitting. Phys Earth Planet Inter 151, 206–222. doi:10.1016/j.pepi.2005.03.003

Long, M.D, van der Hilst, R.D (2006) Shear wave splitting from local events beneath the Ryukyu arc: Trench-parallel anisotropy in the mantle wedge. Phys Earth Planet Inter 155, 300–312. doi:10.1016/j.pepi.2006.01.003

Loveless, J.P, Meade, B.J (2011) Spatial correlation of interseismic coupling and coseismic rupture extent of the 2011 M_w=9.0 Tohoku-oki earthquake. Geophys Res Lett **38**. Art No L17306, doi:10.1029/2011GL048561

Luo, H, Wang, K (2021) Postseismic geodetic signature of cold forearc mantle in subduction zones. Nat Geosc 14, 104–109. doi:10.1038/s41561-020-00679-9

Manea, M, Manea, V.C (2011) Curie point depth estimates and correlation with subduction in Mexico. Pure Appl Geophys 168, 1489–1499. doi:10.1007/s00024-010-0238-2

Mann, M.E, Abers, G.A, Crosbie, K, Creager, K, Ulberg, C, Moran, S, Rondenay, S (2019) Imaging subduction beneath Mount St. Helens: Implications for slab dehydration and magma transport. Geophys Res Lett 46, 3163–3171. doi:10.1029/2018GL081471

Manthilake, G, Koga, K.T, Peng, Y, Mookherjee, M (2021) Halogen bearing amphiboles, aqueous fluids, and melts in subduction zones: Insights on halogen cycle from electrical conductivity. J Geophys Res: Solid Earth **126**. Art No e2020JB021339, doi:10.1029/2020JB021339

Marcaillou, B, Spence, G, Wang, K, Collot, J-Y, Ribodetti, A (2008) Thermal segmentation along the

N. Ecuador–S. Columbia margin (1–4°N): Prominent influence of sedimentation rate in the trench. Earth Planet Sci Lett 272, 296–308. doi:10.1016/j.epsl.2008.04.049

Marschall, H.R, Schumacher, J.C (2012) Arc magmas sourced from mélange diapirs in subduction zones. Nat Geosc 5, 862–867. doi:10.138/ngeo1634

Martindale, M, Skora, S, Pickles, J, Elliott, T, Blundy, J, Avanzinelli, R (2013) High pressure phase relations of subducted volcaniclastic sediments from the west Pacific and their implications for the geochemistry of Mariana arc magmas. Chem Geo 342, 94–109

Mazza, S.E, Stracke, A, Gill, J.B, Kimura, J-I, Kleine, T (2020) Tracing dehydration and melting of the subducted slab with tungsten isotopes in arc lavas. Earth Planet Sci Lett **530**. Art No 115942, doi:10.1016/j.epsl.2019.115942

McCormack, K, Wirth, E.A, Long, M.D (2013) B-type olivine fabric and mantle wedge serpentinization beneath the Ryukyu arc. Geophys Res Lett 40, 1697–1702. doi:10.1002/grl.50369

Merkulova, M, Muñoz, M, Vidal, O, Brunet, F (2016) Role of iron content on serpentinite dehydration depth in subduction zones: Experiments and thermodynamic modeling. Lithos 264, 441–452. doi:10.1016/j.lithos.2016.09.007

Molnar, P, England, P (1990) Temperature, heat flux, and frictional stress near major thrust faults. J Geophys Res: Solid Earth 95, 4833–4856. doi:10.1029/JB095iB04p04833

Mookherjee, M, Capitani, G.C (2011) Trench parallel anisotropy and large delay times: Elasticity and anisotropy of antigorite at higher pressures. Geophys Res Lett **38**. Art No L09315, doi:10.1029/2011GL047160

Morishige, M (2022) The thermal structure of subduction zones predicted by plate cooling models with variable thermal properties. Geophys J Int 229, 1490–1502. doi:10.1093/gji/ggac008

Morishige, M, Honda, S (2013) Mantle flow and deformation of subducting slab at a plate junction. Earth Planet Sci Lett 365, 132–142. doi:10.1016/j.epsl.2013.01.033

Morishige, M, van Keken, P.E (2014) Along-arc variation in the 3-D thermal structure around the junction between the Japan and Kurile arcs. Geochem Geophys Geosys 15, 2225–2240. doi:10.1002/2014GC005394

Morishige, M, van Keken, P.E (2017) Along-arc variation in short-term slow slip events caused by 3-D fluid migration in subduction zones. J Geophys Res: Solid Earth 122, 1434–1448. doi:10.1002/2016JB013091

Müller, R.D, Sdrolias, M, Gaina, C, Roest, R.W (2008) Age, spreading rates, and spreading asymmetry of the world's ocean crust. Geochem Geophys Geosys **9**. Art No Q04006, doi:10.1029/2007GC001743

Muto, J, Shibazaki, B, Iinuma, T, Ito, Y, Ohta, Y, Miura, S, Nakai, Y (2016) Heterogeneous rheology controlled postseismic deformation of the 2011 Tohoku-Oki earthquake. Geophys Res Lett 43, 4971–4978. doi:10.1002/2016GL068113

Muto, J, Moore, J.D.P, Barbot, S, Iinuma, T, Ohta, Y, Iwamori, H (2019) Coupled afterslip and transient flow after the 2011 Tohoku earthquake. Sci Adv **5**. Art No eaaw1164, doi:10.1126/sciadv.aaw1164

Nagaya, T, Walker, A.M, Wookey, J, Wallis, S.R, Ishii, K, Kendall, J-M (2016) Seismic evidence for flow in the hydrated mantle wedge of the Ryukyu subduction zone. Sci Rep **6**. Art No 29981, doi:10.1038/srep29981

Nakajima, J, Hasegawa, A (2004) Shear-wave polarization anisotropy and subduction-induced flow in the mantle wedge of northeastern Japan. Earth Planet Sci Lett 225, 365–377. doi:10.1016/j.epsl.2004.06.011

Nakajima, J, Hada, S, Hayami, E, Uchida, N, Hasegaswa, A, Yoshioka, S, Matsuzawa, T, Umino, N (2013) Seismic attenuation beneath northeastern Japan: Constraints on mantle dynamics and arc magmatism. J Geophys Res: Solid Earth 118, 5838–5855. doi:10.1002/2013JB010388

Ohde, A, Otsuka, H, Kioka, A, Ashi, J (2018) Distribution and depth of bottom-simulating reflectors in the Nankai subduction zone. Earth Planets Space **70**. Art No 60, doi:10.1186/s40623-018-0833-5

Okubo, Y, Matsunaga, T (1994) Curie point depth in northeast Japan and its correlation with regional thermal structure and seismicity. J Geophys Res: Solid Earth 99, 22363–22371. doi:10.1029/94JB01336

Padrón-Navarta, J.A, Tommasi, A, Garrido, C.J, Sánchez-Vizcaíno, V.L, Gómez-Pugnaire, M.T, Jabaloy, A, Vauchez, A (2010) Fluid transfer into the mantle wedge controlled by high-pressure hydrofracturing in the cold top-slab mantle. Earth Planet Sci Lett 297, 271–286. doi:10.1016/j.epsl.2010.06.029

Pang, G, Abers, G.A, van Keken, P.E (2023) Focusing effects of teleseismic wavefields by the subducting plate beneath Cascadia. J Geophys Res: Solid Earth **128**. Art No e2022JB025486, doi:10.1029/2022JB025486

Peacock, S.M (2001) Are the lower planes of double seismic zones caused by serpentine dehydration in subducting oceanic mantle? Geology 29, 299–302. doi:10.1130/0091-7613(2001)029<0299:ATLPOD>2.0.C

Peacock, S.M (2020) Advances in the thermal and petrologic modeling of subduction zones. Geosphere 16, 936–952. doi:10.1130/GES02213.1

Peacock, S.M, Wang, K (2021) On the stability of talc in subduction zones: A possible control on the maximum depth of decoupling between subducting plate and mantle wedge. Geophys Res Lett **48**. Art No e2021GL094889, doi:10.1029/2021GL094889

Peña, C, Heidback, O, Moreno, M, Bedford, J, Ziegler, M, Tassara, A, Oncken, O (2020) Impact of power-law rheology on the viscoelastic relaxation pattern and afterslip distribution following the 2010 Mw 8.8 Maule earthquake. Earth Planet Sci Lett **542**. Art No 116292, doi:10.1016/j.epsl.2020.116292

Piccoli, F, Vitale Brovarone, A, Beyssac, O, Martinez, I, Ague, J.J, Chaduteau, C (2016) Carbonation by fluid-rock interactions at high-pressure conditions: Implications for carbon cycling in subduction zones. Earth Planet Sci Lett 445, 146–158. doi:10.1016/j.epsl.2016.03.045

Pollack, H.N, Hurter, S.J, Johnson, J.R (1993) Heat flow from Earth's interior: Analysis of the global data set. Rev Geophys 31, 267–280. doi:10.1029/93RG01249

Pommier, A, Evans, R.L (2017) Constraints on fluids in subduction zones from electromagnetic data. Geosphere 13, 1026–1041. doi:10.1130/GES01473.1

Pommier, A, Williams, Q, Evans, R.L, Pal, I, Zhang, Z (2019) Electrical investigations of natural lawsonite and application to subduction contexts. J Geophys Res: Solid Earth 124, 1430–1442. doi:10.1029/2018JB016899

Portner, D.E, Hayes, G.P (2018) Incorporating teleseismic tomography data into models of upper mantle slab geometry. Geophys J Int 215, 325–332. doi:10.1093/gji/ggy279

Pozgay, S.H, Wiens, D.A, Conder, J.A, Shiobara, H, Sugioka, H (2009) Seismic attenuation tomography of the Mariana subduction system: Implications for thermal structure, volatile distribution, and slow spreading dynamics. Geochem Geophys Geosys **10**. Art No Q04X05, doi:10.1029/2008GC002313

Prakash, A, Holyoke III, C.W, Kelemen, P.B, Kirby, S.H, Kronenberg, A.K, Lamb, W.M (2023) Carbonates and intermediate-depth seismicity: Stable and unstable shear in altered subducting plates and overlying mantle. Proc Nat Acad Sci **120**. Art No e2219076120, doi:10.1073/pnas.2219076120

Raleigh, C.B, Paterson, M.S (1965) Experimental deformation of serpentinite and its tectonic implications. J Geophys Res: Solid Earth 70, 3965–3985. doi:10.1029/JZ070i016p03965

Reynard, B (2013) Serpentine in active subduction zones. Lithos 178, 171–185. doi:10.1016/j.lithos.2012.10.012

Rogers, G, Dragert, H (2003) Episodic tremor and slip on the Cascadia subduction zone: The chatter of silent slip. Science 300, 1942–1943. doi:10.1126/science.1084783

Rondenay, S, Abers, G.A, van Keken, P.E (2008) Seismic imaging of subduction zone metamorphism. Geology 36, 275–278. doi:10.1130/G24112A.1

Rüpke, L.H, Phipps Morgan, J, Hort, M, Connolly, J.A.D (2004) Serpentine and the subduction zone water cycle. Earth Planet Sci Lett 223, 17–34. doi:10.1016/j.epsl.2004.04.018

Rustioni, G, Audetat, A, Keppler, H (2021) The composition of subduction zone fluids and the origin of the trace element enrichment in arc magmas. Contrib Min Petrol **176**. Art No 51, doi:10.1007/s00410-021-01810-8

Rychert, C.A, Fischer, K.M, Abers, G.A, Plank, T, Syracuse, E, Protti, J.M, Gonzalez, V, Strauch, W (2008) Strong along-arc variations in attenuation in the mantle wedge beneath Costa Rica and Nicaragua. Geochem Geophys Geosys **9**. Art No Q10S10, doi:10.1029/2008GC002040

Sacks, I.S (1968) Distribution of absorption of shear waves in South America and its tectonic significance. Carnegie Inst Year Book 67, 339–344. https://archive.org/details/yearbookcarne67196768carn

Saita, H, Nakajima, J, Shiina, T, Kimura, J-I (2015) Slab-derived fluids, fore-arc hydration, and sub-arc magmatism beneath Kyushu, Japan. Geophys Res Lett 42, 1685–1693. doi:10.0112/2015GL063084

Salmi, M.S, Johnson, P.J, Harris, R.N (2017) Thermal environent of the Southern Washington region of the Cascadia subduction zone. J Geophys Res: Solid Earth 122, 5852–5870. doi:10.1002/2016JB013839

Seno, T (1977) The instantaneous rotation vector of the Philippine sea plate relative to the Eurasian plate. Tectonophysics 42, 209–226. doi:10.1016/0040-1951(77)90168-8

Seno, T, Maruyama, S (1984) Paleogeographic reconstruction and origin of the Philippine Sea. Tectonophysics 102, 53–84. doi:10.1016/0040-1951(84)90008-8

Shelly, D.R, Beroza, G.C, Ide, S, Nakamula, S (2006) Low-frequency earthquakes in Shikoku, Japan, and their relationship to episodic tremor and slip. Nature 442, 188–191. doi:10.1038/nature04931

Shiina, T, Nakajima, J, Matsuzawa, T (2013) Seismic evidence for high pore pressures in oceanic crust: Implications for fluid-related embrittlement. Geophys Res Lett 40, 2006–2010. doi:10.1002/grl.50468

Shiina, T, Nakajima, J, Matsuzawa, T, Toyokuni, G, Kita, S (2017) Depth variations in seismic velocity in the subducting crust: Evidence for fluid-related embrittlement for intermediate-depth earthquakes. Geophys Res Lett 44, 810–817. doi:10.1002/2016GL071798

Shimoda, G, Kogiso, T (2019) Effect of serpentinite dehydration in subducting slab on isotopic diversity in recycled oceanic crust and its role in isotopic heterogeneity of the mantle. Geochem Geophys Geosys 20, 5449–5472. doi:10.1029/2019GC008336

Shirey, S.B, Wagner, L.S, Walter, M.J, Pearson, D.G, van Keken, P.E (2021) Slab transport of fluids to deep focus earthquake depths – thermal modeling constraints and evidence from diamonds. AGU Advances **2**. Art No e2020AV000304, doi:10.1029/2020AV000304

Sippl, C, Schurr, B, John, T, Hainzl, S (2019) Filling the gap in a double seismic zone: Intraslab seismicity in northern Chile. Lithos **346–347**. Art No 105155, doi:10.1016/j.lithos.2019.105155

Smye, A.J, Jackson, C.R.M, Konrad-Schmolke, M, Hesse, M.A, Parman, S.W, Shuster, D.L, Ballentine, C.J (2017) Noble gases recycled into the mantle through cold subduction zones. Earth Planet Sci Lett 471, 65–73. doi:10.1016/j.epsl.2017.04.046

Springer, M, Förster, A (1998) Heat-flow density across the Central Andean subduction zone. Tectonophysics 291, 123–139. doi:10.1016/S0040-1951(98)00035-3

Stachnik, J.C, Abers, G.A, Christensen, G.A (2004) Seismic attenuation and mantle wedge temperatures in the Alaska subduction zone. J Geophys Res: Solid Earth **109**. Art No B10304, doi:10.1029/2004JGB003018

Suenaga, N, Yoshioka, S, Ji, Y (2021) 3-D thermal regime and dehydration processes around the regions of slow earthquakes along the Ryukyu Trench. Sci Rep **11**. Art No 11251, doi:10.1038/s41598-021-90199-2

Suenaga, N, Yoshioka, S, Matsumoto, T, Ji, Y (2018) Two-dimensional thermal modeling associated with the subduction of the Philippine Sea plate in southern Kyushu, Japan. Tectonophysics 723, 288–296. doi:10.1016/j.tecto.2017.12.017

Suenaga, N, Yoshioka, S, Matsumoto, T, C, M.V, Manea, M, Ji, Y (2019) Two-dimensional thermal modeling of the Philippine Sea plate subduction in central Japan: Implications for gap of low-frequency earthquakes and tectonic tremors. J Geophys Res: Solid Earth 124, 6848–6865. doi:10.1029/2018JB017068

Syracuse, E.M, Abers, G.A (2006) Global compilation of variations in slab depth beneath arc volcanoes and implications. Geochem Geophys Geosys **7**. Art No Q05107, doi:10.1029/2005GC001045

Syracuse, E.M, van Keken, P.E, Abers, G.A (2010) The global range of subduction zone thermal models. Phys Earth Planet Int 183, 73–90. doi:10.1016/j.pepi.2010.02.004

Takei, Y (2017) Effects of partial melting on seismic velocity and attenuation: A new insight from experiments. Ann Rev Earth Planet Sci 45, 447–470. doi:10.1146/annurev-earth-063016-015820

Tanaka, A, Yamano, Y, Yano, Y, Sasada, M (2004) Geothermal gradient and heat flow data in and around Japan (I): Appraisal of heat flow from geothermal gradient data. Earth Planets Space 56, 1191–1194. doi:10.1186/BF03353339

Tian, M, Katz, R.F, Rees Jones, D.W, May, D.A (2019) Devolatilization of subduction slabs, part II: Volatile fluxes and storage. Geochem Geophys Geosys 20, 6199–6222. doi:10.1029/2019GC008489

Tsuno, K, Dasgupta, R, Danielson, L, Righter, K (2012) Flux of carbonate melt from deeply subducted pelitic

sediments: Geophysical and geochemical implications for the source of Central American volcanic arc. Geophys Res Lett **39**. Art No L16307, doi:10.1029/2012GL052606

Uchide, N, Nakajima, J, Wang, K, Takagi, R, Yoshida, K, Nakayama, T, Hino, R, Okada, T, Asano, Y (2020) Stagnant forearc mantle wedge inferred from mapping of shear-wave anisotropy using S-net seafloor seismometers. Nat Comm **11**. Art No 5676, doi:10.1038/s41467-020-19541-y

Utsu, T (1966) Regional differences in absorption of seismic waves in the upper mantle as inferred from abnormal distributions of seismic intensities. Journal of the Faculty of Science, Hokkaido University, ser. VII, 2, 359–374

van Dinther, Y, Preiswerk, L.E, Gerya, T.V (2019) A secondary zone of uplift due to megathrust earthquakes. Pure Appl Geophys 176, 4043–4068. doi:10.1007/s00024-019-02250-z

van Keken, P.E (2003) The structure and dynamics of the mantle wedge. Earth Planet Sci Lett 215, 323–338. doi:10.1016/S0012-821X(03)00460-6

van Keken, P.E, Kiefer, B, Peacock, S.M (2002) High-resolution models of subduction zones: Implications for mineral dehydration reactions and the transport of water to the deep mantle. Geochem Geophys Geosys **3**. Art No 1056, doi:10.1029/2001GC000256

van Keken, P.E, Kita, S, Nakajima, J (2012) Thermal structure and intermediate-depth seismicity in the Tohoku-Hokkaido subduction zones. Solid Earth 3, 355–364. doi:10.5194/se-3-355-2012

van Keken, P.E, Hacker, B.R, Syracuse, E.M, Abers, G.A (2011) Subduction factory: 4. Depth-dependent flux of H_2O from subducting slabs worldwide. J Geophys Res: Solid Earth **116**. Art No B01401, doi:10.1029/2010JB007922

van Keken, P.E, Wada, I, Sime, N, Abers, G.A (2019) Thermal structure of the forearc in subduction zones: A comparison of methodologies. Geochem Geophys Geosys 20, 3268–3288. doi:10.1029/2019GC008334

Ventouzi, C, Papazachos, C, Hatzidimitriou, P, Papaioannou, C, EGALADOS Working Group (2018) Anelastic P- and S- upper mantle attenuation tomography of the southern Aegean Sea subducton area (Hellenic Arc) using intermediate-depth earthquake data. Geophys J Int 215, 635–658. doi:10.1093/gji/ggy292

Vho, A, Lanari, P, Rubatto, D, Hermann, J (2020) Tracing fluid transfers in subduction zones: an integrated thermodynamic and $\delta^{18}O$ fractionation modelling approach. Solid Earth 11, 307–328. doi:10.5194/se-11-307-2020

Vitale Brovarone, A, Beyssac, O (2014) Lawsonite metasomatism: A new route for water to the deep Earth. Earth Planet Sci Lett 393, 275–284. doi:10.1016/j.epsl.2014.03.001

Von Herzen, R, Ruppel, C, Molnar, P, Nettles, M, Nagihara, S, Ekström, G (2001) A constraint on the shear stress at the Pacific-Australian plate boundary from heat flow and seismicity at the Kermadec forearc. J Geophys Res: Solid Earth 106, 6817–6833. doi:10.1029/2000JB900469

Wada, I, He, J (2017) Thermal structure of the Kanto region, Japan **44**, 7194–7202. doi:10.1002/2017GL073597

Wada, I, King, S.D (2015) Dynamics of subducting slabs: Numerical modeling and constraints from seismology, geoid, topography, geochemistry, and petrology. In: Schubert, G (ed.) Treatise on Geophysics (2nd Edition), Volume 7 "Mantle Dynamics" (Bercovici, D (ed.)) pp 339–391. Elsevier, Amsterdam, The Netherlands. doi:10.1016/B978-0-444-53802-4.00132-9

Wada, I, Wang, K (2009) Common depth of slab-mantle decoupling: Reconciling diversity and uniformity of subduction zones. Geochem Geophys Geosys **10**. Art No Q10009, doi:10.1029/2009GC002570

Wada, I, Wang, K, He, J, Hyndman, R.D (2008) Weakening of the subduction interface and its effects on surface heat flow, slab dehydration, and mantle wedge serpentinization. J Geophys Res: Solid Earth **113**. Art No B04402, doi:10.1029/2007JB005190

Wada, I, He, J, Hasegawa, A, Nakajima, J (2015) Mantle wedge flow patterns and thermal structure in Northeast Japan: Effects of oblique subduction and 3-D slab geometry. Earth Planet Sci Lett 426, 76–88. doi:10.1006/j.epsl.2015.06.021

Wang, J, Huang, X, Zhao, D, Yao, Z (2019) Seismic anisotropy evidence for ductile deformation of the forearc lithospheric mantle in subduction zones. J Geophys Res: Solid Earth 124, 7013–7027. doi:10.1029/2018JB016912

Wang, K, Wada, I, Ishikawa, Y (2004) Stresses in the subducting slab beneath southwest Japan and relation with plate geometry, tectonic forces, slab dehydration, and damaging earthquakes. J Geophys Res: Solid Earth **109**. Art No B08304, doi:10.1029/2003JB002888

Wang, L, Wang, D, K, S (2020) Electrical conductivity of talc dehydration at high pressures and temperatures: Implications for high-conductivity anomalies in subduction zones. J Geophys Res: Solid Earth **125**. Art No e2020JB020091, doi:10.1029/2020JB020091

Wei, S.S, Wiens, D.A (2018) P-wave attenuation structure of the Lau back-arc basin and implications for mantle wedge processes. Earth Planet Sci Lett 502, 187–199. doi:10.1016/j.epsl.2018.09.005

Wei, S.S, Wiens, D.A, van Keken, P.E, Cai, C (2017) Slab temperature control on the Tonga double seismic zone and slab mantle dehydration. Sci Adv **3**. Art No e1601755, doi:10.1126/sciadv.1601755

Wells, R, Bukry, D, Friedman, R, Pyle, D, Duncan, R, Haeussler, P, Wooden, J (2014) Geological history of Siletzia, a large igneous province in the Oregon and Washington Coast Range: Correlation to the geomagnetic polarity time scale and implications for a long-lived Yellowstone hotspot. Geosphere 10, 692–719. doi:10.1130/GES01018.1

Wilson, C.R, Spiegelman, M.S, van Keken, P.E, Hacker, B.R (2014) Fluid flow in subduction zones: The role of solid rheology and compaction pressure. Earth Planet Sci Lett 401, 261–274. doi:10.1016/j.epsl.2014.05.052

Yin, Y, Li, C-F, Lu, Y (2021) Estimating Curie-point depths using both wavelet-based and Fourier spectral centroid methods in the western Pacific marginal seas. Geophys J Int 227, 798–812. doi:10.1093/gji/ggab257

Yoo, S, Lee, C (2023) Controls on melt focusing beneath old subduction zones: A case study of northeast Japan. Tectonophysics **851**. Art No 229766, doi:10.1016/j.tecto.2023.229766

Yoshioka, S, Suminokura, Y, Matsumoto, T, Nakajima, J (2013) Two-dimensional thermal modeling of subduction of the Philippine Sea plate beneath southwest Japan. Tectonophysics 608, 1094–1108.

doi:10.1016/j.tecto.2013.07.003
Zhao, D.P, Hasegawa, A, Kanamori, H (1994) Deep structure of the Japan subduction zone as derived from local, regional, and teleseismic events. J Geophys Res: Solid Earth 99, 22313–22329. doi:10.1029/94JB01149